UNIVERSITY OF CALIFORNIA
RIVERSIDE

The Seismotectonics and Seismogenesis of the Main Himalayan Thrust in Nepal and India

A Dissertation submitted in partial satisfaction
of the requirements for the degree of

Doctor of Philosophy

in

Geological Sciences

by

Manuel Matthew Mendoza

December 2021

Dissertation Committee:

Dr. Abhijit Ghosh, Chairperson
Dr. Roby Douilly
Dr. Gareth J. Funning

The Dissertation of Manuel Matthew Mendoza is approved:

Committee Chairperson

University of California, Riverside

Acknowledgments

I would like to begin by first thanking: (1) Shyam S. Rai, a professor at the Indian Institute of Science Education and Research, Pune, who graciously shared the Uttarakhand waveform data used in this dissertation; (2) Our collaborators and the field team who helped to deploy the "NAMASTE" seismic network in Nepal, and collected the data that also went into this dissertation; (3) Iris PASSCAL for providing technical support and instruments needed to carry out our labs research; (4) the National Science Foundation, and the Blanchard and Shawn Biehler scholarships for providing financial support.

With that said, completion of this dissertation is the result of the sum contribution of those who have invested their time and energy into my personal and professional growth. It is with great appreciation and warmth that I acknowledge the following people who have supported me at UC Riverside.

Thank you to Pete Sadler, one of the first professors I met in the Earth Sciences department. In my undergraduate, I feel very fortunate to have acquired much of my geology skills and knowledge through the courses he taught. In my graduate training, his high expectations and valuable feedback helped propel expectations of myself to new heights. His door was always open to discuss any questions that I had regarding research, and those that related to the hidden curriculum of academia.

Thank you to Harry Green who welcomed me to work in his Tectonophysics Lab for a brief time in my undergrad. Harry's great prowess as a scientist, combined with such kindness, made him one of my earlier role models. He taught me the importance of being "emotionally invested" in research, a key ingredient to success that I struggled to find early

on. I thank him for believing in me even in times when I did not believe in myself, and for caring about my future. I wish he could show him how much progress I made. May he rest in peace.

Next, thank you to David Oglesby for having such an impact on my undergraduate and graduate learning in the realm of geophysics. He helped me get the ball rolling when I first considered graduate school at UCR and has been supportive ever since. His kindness, wisdom, and excellent sense of humor always uplifted my spirits, especially during some of the more stressful times.

Gareth Funning has also played an integral role in my time at UC Riverside. I thank him for his critical and constructive feedback over the development of this dissertation, helping it be the best that it can be. Further, the advice/knowledge he has shared over the years on navigating through graduate school, and beyond, has been invaluable.

I thank Roby Douilly for lending his exceptional seismological expertise which, most notably, improved the quality of my earthquake catalogs. The discussions we had helped me to overcome important technical problems that I faced in the final years of my PhD. Moreover, I am more diligent going forward when it comes to scrutinizing uncertainties and sources of error in my research.

One other person I would like to thank for being an excellent mentor and role model is Heather Ford. I am incredibly grateful for all the time, advice, and care she has invested into helping me succeed in graduate school. There is no doubt in my mind that completion of this dissertation and the next moves in my career, would have been significantly more difficult to obtain, if not for her support.

Of course, it goes without saying that I express a very special thank you to my advisor and friend, Abhijit Ghosh. Being a new professor at UCR, I would argue that Abhi took a gamble by welcoming me as one of his first undergraduate student researchers into his lab. I would say again he took an even bigger gamble by encouraging me to continue working with him in graduate school! Nonetheless, I thank Abhi for seeing and nurturing my potential as a seismologist from the very beginning, despite the many struggles I faced. Further, he provided the right amount of push and mentorship that has led to much of the success I have now, and will continue to gain going forward. Our one-on-one talks and adventures out in the field will stay with me for a very long time. The dissertation that I am proud to present here, is in large part, a reflection of what he has taught me. It has been a pleasure to grow with him in our own academic roles over the years, and to do some pretty cool science – I look forward to our future collaborations, wherever they may go.

Finally, to the many other colleagues and friends that I have gained throughout my time at UC Riverside; I wish I could name you all and write a page or two for each of you here. Thank you for all your help with my research, and for keeping me sane with all the fun times. I hope that I was able to return the favor. A special thank you to Kenny Ryan who planted the seed in my mind that I should consider graduate school, and for also telling me to "hurry up" from time to time after I started. I am grateful. Also, to Christodoulos Kyriakopoulos, thank you for all the encouragement—I apologize again for shooting the nerf dart into your office while you were busy working (Jennifer Tarnowski made me do it).

The text of this dissertation, in part, is a reprint of the material as it appears in: (1) Mendoza, M. M., Ghosh, A., Karplus, M. S., Klemperer, S. L., Sapkota, S. N., Adhikari, L. B., and Velasco, A. (2019). Duplex in the Main Himalayan Thrust illuminated by aftershocks of the 2015 Mw 7.8 Gorkha earthquake. Nature Geoscience, 12(12), 1018-1022; and (2) Mendoza, M. M., Ghosh, A., and Rai, S. S. (2016). Dynamic triggering of small local earthquakes in the central Himalaya. Geophysical Research Letters, 43(18), 9581-9587. The co-author Dr. Abhijit Ghosh listed in those publications directed and supervised the research which forms the basis for this dissertation.

To my significant other, Megan Meyer, thank you for all the happiness and unwavering support. From applying to college to submitting my post-doc applications, and everything in between, you were there to help keep me afloat through it all. To my younger siblings, Andrew and Britney Mendoza, thank you for being one of the biggest reasons why I gathered the courage to aim so high. I wanted to break down ceilings to show you what was possible when it came to pursuing your dreams, especially when positioned in very unfavorable circumstances. Tread your own path and do not stop. To my mother, Cindy Mendoza, this journey began because of you. The instability of homelessness does not necessarily favor a child to make it this far, but somehow you were able to help make it happen as a single mother. You provided the love and freedom that allowed my siblings and I to pursue whatever it is that made us happy, and without expecting anything in return. In my first year of college I was not sure how I would overcome poor grades while working and taking you to the doctors when you were sick; but, seeing your strength during those times is when I developed perhaps my most powerful trait—grit. Some good came out of all the bad. I combined this with the kindness you raised us with, and am now more prepared to have the positive impact I always wanted. You are amazing and have done a wonderful job.

I love you all from the bottom of my heart. Thank you.

ABSTRACT OF THE DISSERTATION

The Seismotectonics and Seismogenesis of the Main Himalayan Thrust in Nepal and India

by

Manuel Matthew Mendoza

Doctor of Philosophy, Graduate Program in Geological Sciences
University of California, Riverside, December 2021
Dr. Abhijit Ghosh, Chairperson

The Main Himalayan Thrust (MHT) is the cardinal fault (décollement) that accommodates most of the relative convergence between the Indian plate and Eurasian plate. This collision led to a series of complex faulting and folding events that have since created the Himalaya. Consequently, this region has prompted seismological studies to discern the physical properties of the MHT, and characterize deformation processes taking place above and below it. However, probing the Himalayan subsurface in high fidelity is challenging, requiring the deployment of large, dense seismic networks above various, and structurally distinctive segments of the MHT. This is necessary to capture earthquakes across a range of magnitudes (micro to great), locate their hypocenters accurately, and make reliable interpretations accordingly. In this dissertation, we use waveform data from two well-distributed seismic networks temporarily deployed in central Nepal and Uttarakhand, India, to investigate the behavior of seismicity, their influence on one another, and their relationship to Himalayan tectonics.

After the 2015 Mw 7.8 Gorkha earthquake, we deployed the "NAMASTE" seismic network to capture the prolific sequence of aftershocks. From 2005-2008, the Uttarakhand seismic network blanketed a segment of the MHT that is considerably more seismically quiet due to the ongoing and heightened buildup of tectonic strain. From these data sets we develop high-quality earthquake catalogs using a combination of traditional and novel techniques. Focal mechanisms were also computed to determine the orientation and slip direction of structures delineated by their locations.

At shallow depths, we find a duplex structure in both regions, and construct a refined geometric model of the MHT incorporating this structure. At greater depths beneath Uttarakhand, specifically, we provide evidence of earthquakes near the Moho that may be associated with flexural bending of the Indian lithosphere or localized processes. Lastly, we document the first observed instance of remotely triggered earthquakes in Uttarakhand, reaffirming the notion that faults here are critically stressed, and governed by both static and dynamic processes. We therefore stress the importance of using these observations to help constrain other geological and geophysical models that investigate deformation, the behavior of large earthquakes, and high seismic hazard along the Himalaya.

Contents

List of Figures

List of Tables

Chapter 1

Introduction

A hallmark feature of the convergence between the Indian and Eurasian tectonic plates is the Himalayan arc, a ∼2,400 km-long mountain range constructed by complex faulting and folding, cohabitated by some of the most devastating earthquakes on Earth (Figure 1.1). The Main Himalayan Thrust (MHT) fault is a shallowly dipping décollement demarcating the two plates. Major surface breaching, steeply-dipping splay faults that root from it are—from south to north—the Main Frontal Thrust (MFT), Main Boundary Thrust (MBT), and Main Central Thrust (MCT) faults. Typically, the MFT and MBT are seismically quiet, and usually slip during great (Mw≥8) earthquakes that rupture the frictionally locked portion of the MHT towards the surface (Bollinger et al., 2016; Lavé et al., 2005; Kumar et al., 2010; Hetényi et al., 2016; S. Sapkota et al., 2013; Bilham, 2019). Events of this magnitude a rare, occurring on centennial or even millennial timescales (e.g., Bilham, 2019; Dal Zilio et al., 2019; Stevens and Avouac, 2016; S. Sapkota et al., 2013). The MCT, which juxtaposes the meta-sedimentary Lesser Himalayan rock to the south

with higher-grade Greater Himalayan rock to the north, is the oldest of the three major splay faults and is argued to be largely dormant (Ni and Barazangi, 1984). This prompts an important question—given the seismic lull along these thrusts, how is the Himalayan arc undergoing tectonic deformation and governing earthquake processes? Pursuing this umbrella question has critical implications towards our understanding of mega-thrust faults in general, and, most importantly, the high seismic hazard they pose towards vulnerable population centers.

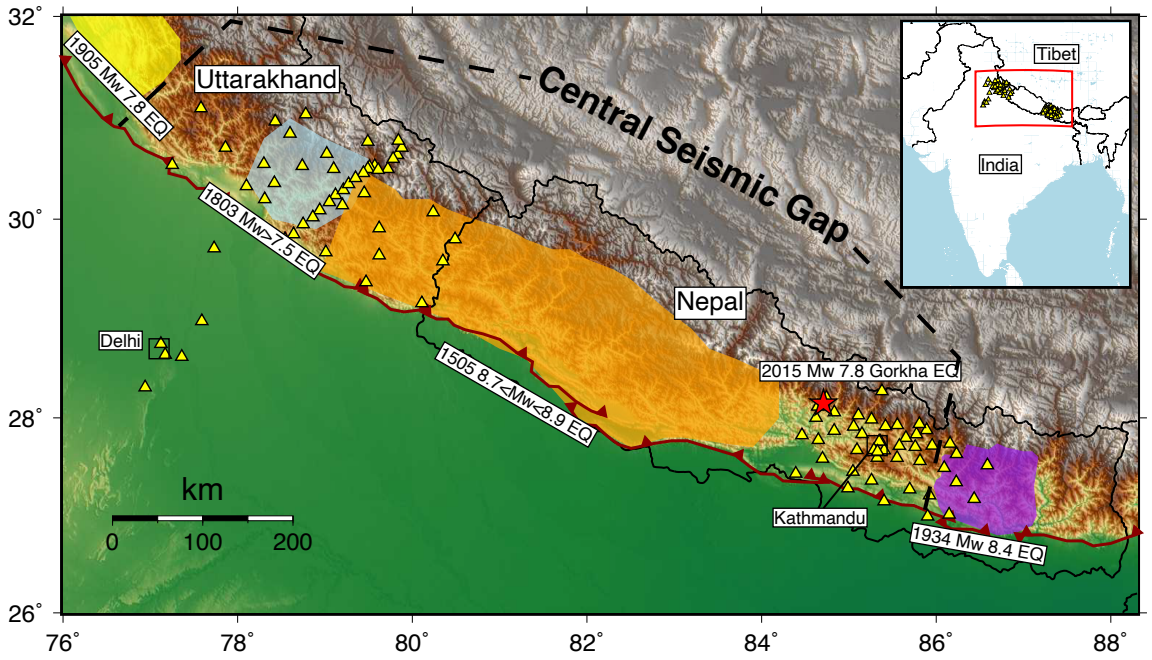

Figure 1.1: Elevation map of the Himalayas and surrounding region showing the station distribution (yellow triangles) of the two networks used in this dissertation: the NAMASTE network in Nepal (Karplus et al., 2020), and the Uttarakhand network in Indian (Mahesh et al., 2013). The dark-red barbed line represents the surface trace and dip direction of the MFT—later chapters show other major surface-breaching faults such as the MBT and MCT. Colored polygons represent the inferred rupture areas of large ($7 \leq$ Mw ≤ 9) historic earthquakes along the MHT as compiled by Bilham (2019) from various sources. The red star shows the location of the most recent large earthquake in the region, the 2015 Mw 7.8 Gorkha earthquake. Roughly situated between the 1934 and 1905 rupture areas is the central seismic gap, where multiple unruptured segments of the MHT are inferred to be sufficiently mature to host a M8 or greater earthquake.

The shallow and locked portion of the MHT is recognized as being comprised of various segments, or zones, defined by the spatial extent of previous large earthquake ruptures (Figure 1.1). Each historical rupture zone is at a different state in their seismic cycle based on the elapsed time since their last major (M7) or great (M8+) earthquake. For example, some segments are early in their cycle, while others are late/overdue in producing their next earthquake. The general timing and magnitude (size) of the next destructive Himalayan earthquake is dependent on how much elastic strain any one segment has accumulated since hosting its last earthquake of equivalent magnitude. The most concerning segments of the MHT reside in what is commonly referred to as the 'central seismic gap', where others have inferred there is considerable accumulated slip potential—at least 10 m of slip deficit—to drive a great plate boundary-type event (e.g., Bilham, 2019; Dal Zilio et al., 2019; Stevens and Avouac, 2016; Mugnier et al., 2013; C. Rajendran and K. Rajendran, 2005). As shown in Figure 1.1, this gap is up to 800-km in length, stretching from the rupture zones of the 1905 and 1833 Mw =7.8 earthquakes. Within the gap, felt-intensity data reports (Szeliga et al., 2010; S. Martin and Szeliga, 2010; Bilham and Nicholas Ambraseys, 2005; NN Ambraseys and Douglas, 2004) and paleoseismic studies (Malik et al., 2017; Hossler et al., 2016; Yule et al., 2006) provide evidence of three notably large pre-twentieth century earthquakes: from west to east, a Mw 7.6-8.0 earthquake in 1803; a Mw 8.7-8.9 earthquake in 1505; and a Mw 7.7 earthquake in 1833 (Figure 1.1). Given the location, magnitude, and rupture extent, it is hypothesized that the 2015 Mw 7.8 Gorkha, Nepal earthquake was a repeat of the 1833 earthquake (Mencin et al., 2016; S. S. Martin, Hough, and Hung, 2015). Both earthquakes are inferred to be incomplete ruptures for not breaking

the up-dip limit of the MHT nor producing significant afterslip (Bilham, 2019; Mencin et al., 2016). If that were not the case, and the shallower portion of the MHT had accumulated elastic strain to a critical level, it is possible that the 1833 and 2015 earthquakes would have completely ruptured up to the frontal thrusts as a larger event. Such a scenario is akin to the 1505 earthquake (Yule et al., 2006), whose estimated size and rupture extent—although debated—fills most of the central seismic gap. It is important to note, however, that these earthquakes do not represent the largest events possible along the Himalayan arc (Stevens and Avouac, 2016). Further, large uncertainty likely exists in the available historical data, and can lead to (honest) misinterpretations of those earthquakes. Nonetheless, historically large earthquakes hold valuable clues for those that will occur next in the Himalayas.

Through this dissertation we investigate two segments of the MHT within the central seismic gap, where—for M7 or greater earthquakes—one is very early in its seismic cycle, and the other is late. At the eastern end, the 2015 Mw 7.8 Gorkha earthquake unzipped the lower locked portion of the MHT, releasing up to 8 m of peak coseismic slip (Elliott et al., 2016). This earthquake and its many large aftershocks tragically resulted in the loss of over 9,000 lives, injured 22,000 and left 3.5 million people displaced from their homes (Bilham, 2019). If this event had completely ruptured the MHT towards the surface, the scenario would likely have been much worse. Conversely, at the western end of the seismic gap, the densely populated Indian state of Uttarakhand (i.e. Kumaon-Garhwal) is overdue to experience a similar (or larger) devastating plate boundary earthquake. Convergence rate estimates and dates of historic earthquakes in this area indicate the MHT has accumulated 10 meters of slip deficit, which is enough to produce a M8 or greater earthquake (Bilham,

2019). With contemporary advances in seismic monitoring, we are in a prime position to learn from these two segments of the MHT that are at different endmembers in their earthquake cycle. An investigation into each has the potential to offer unique insight into the seismogenic and seismotectonic conditions that govern large Himalayan earthquakes and deformation throughout arc.

In pursuit of these goals, we develop two high-resolution earthquake catalogs from dense local seismic networks in central Nepal and Uttarakhand. The 11-month long Nepal catalog contains 8,292 relocated Gorkha earthquake aftershocks from a collaborative rapid response seismic network that blanketed the rupture area. The 20-month long Uttarakhand catalog contains 736 relocated (non-aftershock type) earthquakes from a similar sized, network operated by the Council of Scientific and Industrial Research National Geophysical Research Institute and the Wadia Institute of Himalayan Geology (Mahesh et al., 2013). The details of these two networks are described in the subsequent chapters. In both catalogs we examine the spatiotemporal distribution of seismicity, their source parameters, and the earthquakes waveforms themselves, to characterize structural features and evaluate stress heterogeneities in the Himalaya. Specifically, in Chapter I use the Gorkha earthquake aftershock locations and their focal mechanisms to delineate a system of bounded imbricate thrusts faults, known as a duplex. By identifying this structure, we offer an updated geometry model of the MHT in central Nepal, and discuss the implications of such a configuration towards our understanding of Himalayan tectonics and earthquake processes. In Chapter 2, we perform a similar analysis for the Uttarakhand dataset and observe two major characteristics in our earthquake catalog. At shallow depths (¡15 km), seismicity also delineates the

presence of a duplex, indicating that this structure is possibly prevalent across the Himalaya arc. Near the Mohorovicic Discontinuity (or "Moho"), at 40-60 km depths, we observe the existence of sparse seismicity where they are thought to be incapable of occurring. We use focal mechanisms to systematically interpret various faulting styles that might be expressed in the lower crust and lithospheric mantle. This analysis provides insight into dynamic processes allowing for brittle failure to occur at these depths beneath the Himalaya, or in other subduction zone environments. In chapter 3, the Uttarakhand dataset is exploited further, where we present findings on the first documented case of the remote earthquake triggering phenomenon in Himalaya. We observe a heightened and sustained increase in the local background seismicity rate during and after the passage of large teleseismic surface waves produced by the 2008 Mw 8.5 Sumatra earthquake—an event that took place 4500 away. The occurrence of both dynamic and delayed earthquake triggering in a segment of the MHT considered to be in a seismic lull suggests that faults here are critically stressed. We explore primary and secondary driving processes at play and relate them towards our understanding of stress perturbations on the earthquake cycle in the Himalayas. Finally, in Chapter 4, we summarize findings obtained over the development of this dissertation, in the context of two spatially distinct Himalayan segments within the central seismic gap. More importantly, I discuss what future works need to be carried out to further our knowledge on the tectonics, earthquakes, and seismic hazard of the Himalayas.

Bibliography

Ambraseys, NN and J Douglas (2004). "Magnitude calibration of north Indian earthquakes". In: *Geophysical Journal International* 159.1, pp. 165–206.

Bilham, Roger (2019). "Himalayan earthquakes: a review of historical seismicity and early 21st century slip potential". In: *Geological Society, London, Special Publications* 483.1, pp. 423–482.

Bilham, Roger and Nicholas Ambraseys (2005). "Apparent Himalayan slip deficit from the summation of seismic moments for Himalayan earthquakes, 1500–2000". In: *Current science*, pp. 1658–1663.

Bollinger, L et al. (2016). "Slip deficit in central Nepal: Omen for a repeat of the 1344 AD earthquake?" In: *Earth, Planets and Space* 68.1, pp. 1–12.

Dal Zilio, Luca et al. (2019). "Bimodal seismicity in the Himalaya controlled by fault friction and geometry". In: *Nature communications* 10.1, pp. 1–11.

Elliott, JR et al. (2016). "Himalayan megathrust geometry and relation to topography revealed by the Gorkha earthquake". In: *Nature Geoscience* 9.2, pp. 174–180.

Hetényi, György et al. (2016). "Segmentation of the Himalayas as revealed by arc-parallel gravity anomalies". In: *Scientific reports* 6.1, pp. 1–10.

Hossler, T et al. (2016). "Surface ruptures of large Himalayan earthquakes in Western Nepal: Evidence along a reactivated strand of the Main Boundary Thrust". In: *Earth and Planetary Science Letters* 434, pp. 187–196.

Karplus, Marianne S et al. (2020). "A rapid response network to record aftershocks of the 2015 M 7.8 Gorkha earthquake in Nepal". In: *Seismological Research Letters* 91.4, pp. 2399–2408.

Kumar, Senthil et al. (2010). "Paleoseismological evidence of surface faulting along the northeastern Himalayan front, India: Timing, size, and spatial extent of great earthquakes". In: *Journal of Geophysical Research: Solid Earth* 115.B12.

Lavé, Jérôme et al. (2005). "Evidence for a great medieval earthquake (˜ 1100 AD) in the central Himalayas, Nepal". In: *Science* 307.5713, pp. 1302–1305.

Mahesh, P et al. (2013). "One-dimensional reference velocity model and precise locations of earthquake hypocenters in the Kumaon–Garhwal himalaya". In: *Bulletin of the Seismological Society of America* 103.1, pp. 328–339.

Malik, Javed N et al. (2017). "Paleoseismic evidence of the CE 1505 (?) and CE 1803 earthquakes from the foothill zone of the Kumaon Himalaya along the Himalayan Frontal Thrust (HFT), India". In: *Tectonophysics* 714, pp. 133–145.

Martin, Stacey and Walter Szeliga (2010). "A catalog of felt intensity data for 570 earthquakes in India from 1636 to 2009". In: *Bulletin of the Seismological Society of America* 100.2, pp. 562–569.

Martin, Stacey S, Susan E Hough, and Charleen Hung (2015). "Ground motions from the 2015 M w 7.8 Gorkha, Nepal, earthquake constrained by a detailed assessment of macroseismic data". In: *Seismological Research Letters* 86.6, pp. 1524–1532.

Mencin, David et al. (2016). "Himalayan strain reservoir inferred from limited afterslip following the Gorkha earthquake". In: *Nature Geoscience* 9.7, pp. 533–537.

Mugnier, J-L et al. (2013). "Structural interpretation of the great earthquakes of the last millennium in the central Himalaya". In: *Earth-Science Reviews* 127, pp. 30–47.

Ni, James and Muawia Barazangi (1984). "Seismotectonics of the Himalayan collision zone: Geometry of the underthrusting Indian plate beneath the Himalaya". In: *Journal of Geophysical Research: Solid Earth* 89.B2, pp. 1147–1163.

Rajendran, CP and Kusala Rajendran (2005). "The status of central seismic gap: a perspective based on the spatial and temporal aspects of the large Himalayan earthquakes". In: *Tectonophysics* 395.1-2, pp. 19–39.

Sapkota, SN et al. (2013). "Primary surface ruptures of the great Himalayan earthquakes in 1934 and 1255". In: *Nature Geoscience* 6.1, pp. 71–76.

Stevens, VL and J-P Avouac (2016). "Millenary Mw¿ 9.0 earthquakes required by geodetic strain in the Himalaya". In: *Geophysical Research Letters* 43.3, pp. 1118–1123.

Szeliga, Walter et al. (2010). "Intensity, magnitude, location, and attenuation in India for felt earthquakes since 1762". In: *Bulletin of the Seismological Society of America* 100.2, pp. 570–584.

Yule, D et al. (2006). "Possible evidence for surface rupture of the Main Frontal Thrust during the great 1505 Himalayan earthquake, far-western Nepal". In: *AGU Fall Meeting Abstracts*. Vol. 2006, S33C–05.

Chapter 2

Duplex in the Main Himalayan Thrust Illuminated by Aftershocks of the 2015 Mw 7.8 Gorkha Earthquake

2.1 Abstract

In April 2015, the lower locked portion of the Main Himalayan Thrust ruptured beneath Nepal, causing the disastrous M_w 7.8 Gorkha earthquake. Elucidating the enigmatic geometry of this plate boundary fault is important for understanding the nucleation and arrest of large earthquake ruptures, as well as the seismic hazard, topography, and tectonics of the Himalaya. Here we interpret the geometry of the Main Himalayan Thrust

from the spatial distribution and rupture patterns of a dynamic sequence of aftershocks following the Gorkha earthquake, which were recorded by a rapidly deployed dense seismic network. We find that the thrust comprises two north-dipping subhorizontal planes that are connected by a system of bounded imbricate thrust faults, known as a duplex. We propose that this duplex acts as an impediment to plate convergence and accommodates tectonic stress along its complex system of faults. Such a prominent structure to the Main Himalayan Thrust is consistent with surface geological studies, but challenges geophysically derived conventional models with simpler geometries.

2.2 Introduction

Through a combination of infrastructure failure and triggered landslides, the 2015 moment magnitude (M_w)7.8 Gorkha earthquake in Nepal killed at least 9,000 people, probably harmed thousands more and left 3.5 million people homeless (Bilham, 2015). Its largest aftershock to the east, the M_w 7.3 Kodari earthquake, occurred 2 wk later, causing more destruction. In a geological instant, the two events effectively unfastened a ∼160 km along-strike length at the lower edge of locked portion of the Main Himalayan Thrust fault (MHT), offering a snapshot into the complex structures that are fostered by the evolving collision between the Indian and Eurasian plates. The plate convergence, at a rate of ∼20 mm/yr (Bilham, Gaur, and Molnar, 2001) is known to produce frequent moderate-size earthquakes and infrequent large damaging earthquakes like this one to accommodate the incremental passage of the Indian plate beneath the Tibetan Plateau (Dal Zilio et al., 2019). Just 240 km southeast of the Gorkha epicenter, the last destructive earthquakes to occur

in the region were the 1934 M_w 8.1 Nepal-Bihar (Figure 2.2) (W.-P. Chen and Molnar, 1977; Bilham, 1995; Ambraseys and Douglas, 2004) and 1833 M∼7.7 earthquakes (Bilham, 1995; Ambraseys and Douglas, 2004). The 1934 event had a similar along-strike rupture length to the Gorkha earthquake, ∼150 km, but unlike the 1833 event, it is inferred to have ruptured to the surface along the trace of the Main Frontal Thrust (MFT) (Sapkota et al., 2013). Although the location and extent of rupture for the 1833 event are poorly constrained (Bilham, 1995), it is hypothesized that the Gorkha event may have been a repeat of the 1833 event that ruptured the same fault segment of the MHT (Bilham, 2019; Mugnier et al., 2017; S. S. Martin, Hough, and Hung, 2015). Judging from the locations of these previous major earthquakes, and because the Gorkha event did not rupture the surface or have substantial up-dip afterslip (J.-P. Avouac et al., 2015; Elliott et al., 2016; Grandin et al., 2015; Gualandi et al., 2017), another future damaging earthquake may occur to relieve accumulating tectonic strain in this shallower fault segment of the Himalaya (Dal Zilio et al., 2019).

Before the 2015 Gorkha earthquake, the National Seismic Network in Nepal, operated by the National Seismological Centre, had 14 short-period seismic stations operating in central and eastern Nepal (L. Adhikari et al., 2015). The centre publishes an earthquake catalogue online including events of local magnitude (M_L) > 4. While this is a critically important effort, additional stations are needed to better constrain the locations and monitor how the Himalayan thrust belt is deforming, while supporting its high topography and storing tectonic strain. Due to the structural complexity and limited data for this region, there are many competing models for the orientation and geometry of the MHT developed

from a variety of geological (Khanal et al., 2015; Robinson and A. J. Martin, 2014; DeCelles et al., 2001; Hubbard et al., 2016; Wobus et al., 2005; Bollinger et al., 2004) and geophysical (Elliott et al., 2016; Duputel et al., 2016; Whipple et al., 2016; Gao et al., 2016; Nábělek et al., 2009; Lemonnier et al., 1999) methods that lack resolution at depth. Six weeks after the Gorkha earthquake, we deployed a dense, 45-station seismic network for 11 mo in central Nepal, called the Nepal Array Measuring Aftershock Seismicity Trailing Earthquake (NAMASTE) Array (Karplus et al., 2015). Extending 222 km east–west and 133 km north–south with an average station spacing of 20 km, our NAMASTE network blanketed the entire rupture area to capture the prolific and dynamic sequence of aftershocks. From this regional network, we developed a robust catalogue containing over 8,000 earthquakes, all relatively relocated using HypoDD (Waldhauser and Ellsworth, 2000) with a local velocity model (Pandey et al., 1995). The tight clustering of earthquake hypocentres illuminates the geometry of the MHT with unprecedented fidelity to depths of ∼30 km (Figure 2.4). In combination with earthquake moment tensors, we show a duplex along the MHT that is consistent with strong geological evidence of a Lesser Himalayan duplex (Khanal et al., 2015; Robinson and A. J. Martin, 2014; DeCelles et al., 2001), reconcile them with three selected studies that present competing geometric models for the MHT in Nepal (Elliott et al., 2016; Hubbard et al., 2016; Nábělek et al., 2009) and relate these structures to the overall seismogenic processes and associated hazards in the Himalaya.

2.3 Methods

Using the Antelope (version 5.8, Boulder Real Time Technologies) software package, P-wave phases were automatically picked by running a short-term average/long-term average (STA/LTA) filter on all stations between 1 and 5 Hz and between 5 and 12 Hz. Candidate phases that did not meet a preset signal-to-noise ratio were discarded. We then used a second automatic algorithm, dbshear (Ross et al., 2016), to detect S-wave arrivals between 5 and 12 Hz to accurately determine hypocentres. Next, P and S phases detected by at least four stations were associated with a preliminary event using a fine three dimensional travel-time grid. Initial events were then relocated by perturbing (inverting) their origins on said grid to refine final locations and produce error estimates. Events that were relocated on the edges of the grid (the Cartesian aperture of the network) were discarded. All parameters used in the detection and location process were finalized once results became consistent with our mini trial catalogue where the equivalent process was exercised visually and manually (for example, by hand-picking arrivals of seismic phases). Lastly, M_L was computed in Antelope for the finalized relocated events.

The 12,613 events that constitute our absolute catalogue were then passed into HypoDD (version 1.3) (Waldhauser and Ellsworth, 2000) to be relatively relocated, but only events that were located with at least five phase arrivals were used. The conjugate gradients method (LSQR) (Paige and Saunders, 1982) was used for relative relocation. Notable parameters in HypoDD (Waldhauser and Ellsworth, 2000) to achieve such tight clustering between event pairs are the following: a minimum of eight catalogue links per event pair, a minimum of eight phase links to define a neighbour and a maximum separation value of 4

km between event pairs. In both location procedures of Antelope and HypoDD (Waldhauser and Ellsworth, 2000) a local velocity model was used (Pandey et al., 1995). This left us with a final earthquake catalogue containing 8,292 events, with local magnitudes varying between –0.3 and 5.1 (Figure 2.1a). A maximum likelihood analysis (Wiemer, 2001) shows that our catalogue is complete above a magnitude of 1.8 and has a b value of 0.8 (Figure 2.1a). Important to note is that for two brief periods—in early September and late December of 2015—our stations began to run out of disk space, resulting in a sudden decrease in aftershock detections; nonetheless, the frequency of aftershocks diminished gradually over time in an Omori law-like manner (Figure 2.1).

To derive a model for the upper and lower planes of the MHT, we excluded the blob of seismicity as well as the sparse seismicity north of our northernmost station (87 km north of the MBT) and south of the southern band of seismicity. The two bands of moderate and diffuse seismicity were then contoured by density. For the densest regions within these contours (black dots in Figure 2.4), we determined two best-fitting straight lines to estimate the dip and depth of the northern and southern planes of the MHT. In this analysis, because we collapsed all the seismicity beneath the NAMASTE array onto a single cross-section perpendicular to the MBT, the strike of these planes is required to be $\sim$292°. Although this method ignores along-strike variability in structure, our simple approach allows us to define representative parameters for the geometrically simple subhorizontal segments of the MHT.

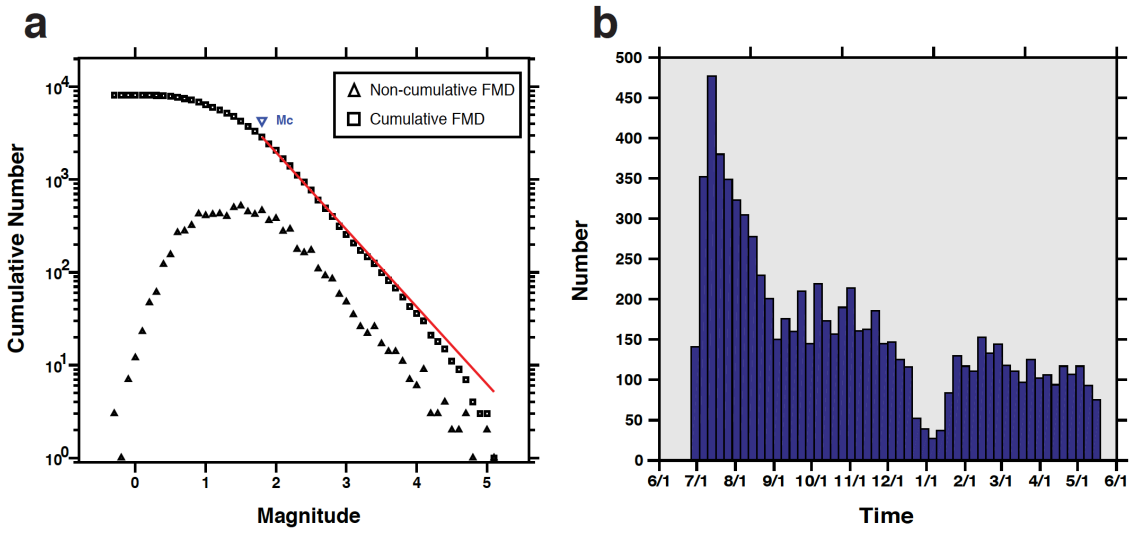

Figure 2.1: **a**, Frequency-Magnitude plot using the maximum-likelihood method to determine a b-value of 0.8, and a magnitude of completeness of 1.8. **b**, Number of earthquakes plotted versus time for the duration of our temporary "NAMASTE" network. The sudden decrease in the frequency of earthquake detections in December 2015 and January 2016 is due to storage disks reaching full capacity.

2.4 Results from the NAMASTE Network

Although the NAMASTE array was deployed 6 wk after the Gorkha earthquake, some features in our 11 mo catalogue are strikingly similar to a catalogue developed by a study that explored the first 45 d of the Gorkha earthquake aftershocks using the Nepal Seismological Network (L. Adhikari et al., 2015). Both catalogues show moderate seismicity between 20 and 48 km northeast of the Main Boundary Thrust (MBT), around where the physiographic transition from Lesser Himalaya to Greater Himalaya begins (Wobus et al., 2005). The catalogues are also similar in showing greatly increased numbers of aftershocks to the north beneath the foothills of the Greater Himalaya. This increased seismicity forms a band that trends from the Gorkha earthquake to the Kodari earthquake, but varies from narrow to broad along-strike (Figure 2.2a), suggesting complex structural controls along

the MHT. The main differences between these two catalogues are that ours contains the aftershock sequence for a much longer duration and is based on our much denser network with better azimuthal coverage using three-component seismometers, allowing us to more precisely locate thousands of micro- to moderate magnitude earthquakes.

In map view, we observe a southern and a northern band of moderate and diffuse seismicity (Figure 2.2a), especially on the western side of our network, making it difficult to constrain the geometry of the MHT in these areas. Within the southern band, an interseismic coupling map based on geodetic data (Ader et al., 2012) (Figure 2.2b) shows a frictionally locked MHT (coupling >0.9) inhibiting post-mainshock brittle failure, and thus indicating an area of ongoing stress buildup (Gualandi et al., 2017; Ader et al., 2012). The northern band of seismicity parallels the coupling contour line of 0.7 (Figure 2.2b), and both undulate along-dip of the MHT from west to east. The area of highest aftershock activity extends from the epicentre of the Gorkha earthquake to slightly east of the Kodari earthquake, predominantly along the northern edge of co-seismic slip (Elliott et al., 2016) (Figure 2.2b), just below the foothills of the Greater Himalaya where considerable post-seismic deformation is inferred to have taken place (J.-P. Avouac et al., 2015; Elliott et al., 2016; Grandin et al., 2015; Gualandi et al., 2017). Thus, seismicity is moderate for 48 km north of the MBT because of high coupling of the MHT. Between 48 and 70 km, seismicity is intense due to coupling decreasing rapidly northeastwards and due to stress loading from the Gorkha earthquake. Then seismicity becomes increasingly sparse north of 70 km (measured from the MBT), where the MHT has been inferred by geodetic data to transition from locked to creeping (Bilham, 2019; Ader et al., 2012; Bettinelli et al., 2006).

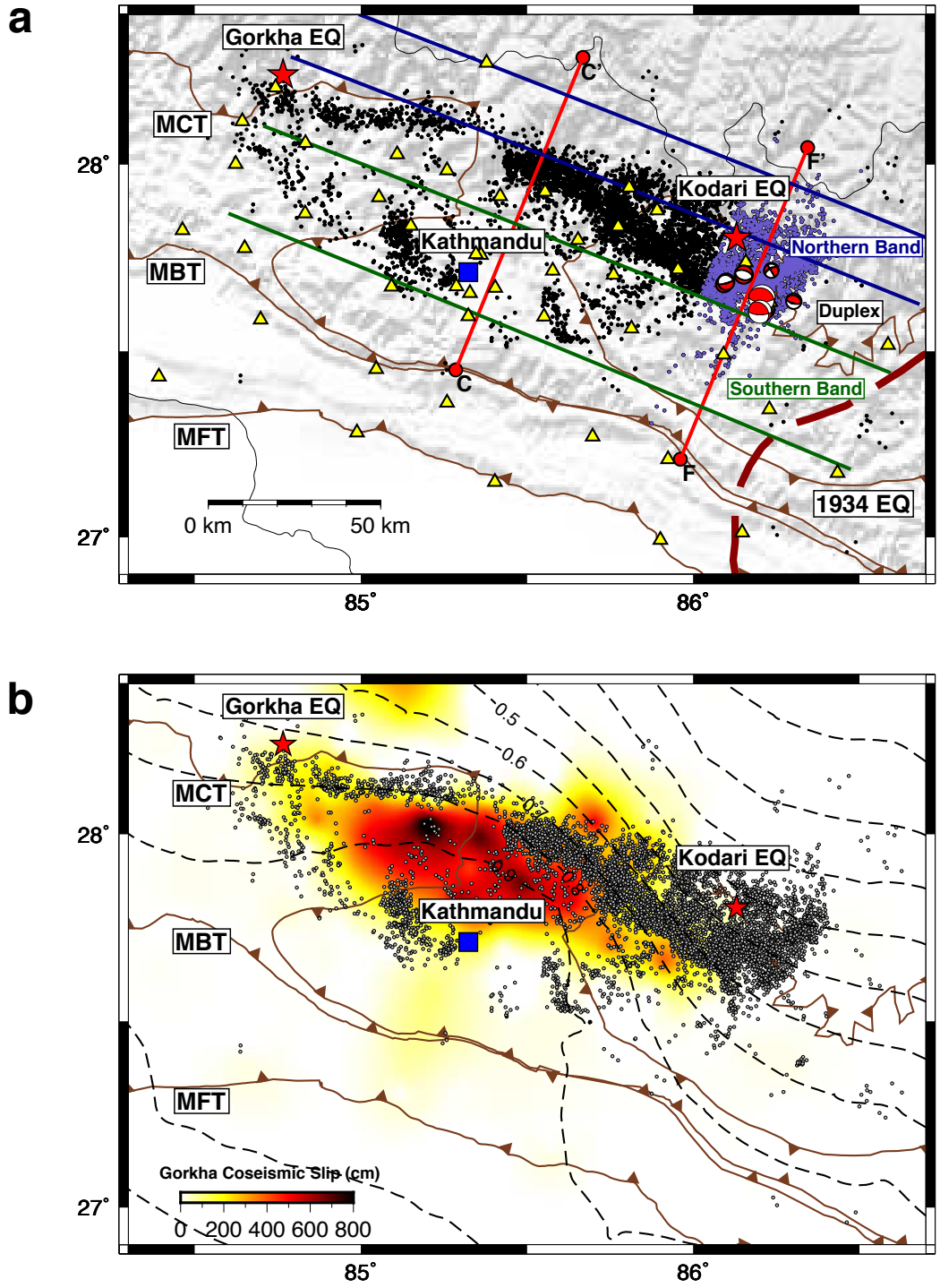
a
Gorkha EQ
C'
MCT
F'
28˚
Kodari EQ
Kathmandu
Northern Band
MBT
Duplex
C
Southern Band
MFT
F
1934 EQ
0 km
50 km
27˚
85˚
86˚
b
Gorkha EQ
0.5
0.6
MCT
28˚
Kodari EQ
Kathmandu
MBT
MFT
Gorkha Coseismic Slip (cm)
0 200 400 600 800
27˚
85˚
86˚

Figure 2.2: Maps of the 2015 Mw 7.8 Gorkha earthquake aftershock sequence in central Nepal. **a**, Greyscale topography overlaid by locations of earthquakes (circles), stations (yellow triangles), major surface thrust faults (dark-brown barbed lines) that sole into the MHT, and the inferred rupture area of the 1934 earthquake (dark-red dashed line) (Ambraseys and Douglas, 2004; L. Adhikari et al., 2015). All events are collapsed onto profile line C–C' for view in cross-section (Figure 2.4a). Events in purple, specifically, are collapsed onto profile line F–F' for view in cross-section (Figure 2.4b) where the duplex is most apparent. We show the most important moment tensors in this area, and not elsewhere, to minimize obstruction of the seismicity distribution—all moment tensors are given in Figure 2.3 and Tables 2.1 and 2.2. There are four distinct style attributes for the moment tensors shown in this study: bold are those we derived here, non-bold are those derived from Bai et al. (2019), blue represent events that occurred on the MHT based on their location, and red represent events that occurred on higher-angle faulting structures. Southern and northern seismicity bands used to constrain the upper and lower planes of the MHT are labelled between the set of blue and green lines, respectively. The along-dip extent of the duplex is labelled between the blue and green lines. **b**, Co-seismic slip (yellow-red) distribution of the 2015 Mw 7.8 Gorkha earthquake (Elliott et al., 2016) overlaid by interseismic coupling contours of the MHT (Ader et al., 2012) (black dashed lines). The locations of the Gorkha and Kodari earthquakes are from Bai et al. (2019). MCT, Main Central Thrust; MBT, Main Boundary Thrust; MFT, Main Frontal Thrust; EQ, earthquake.

2.5 Constraining a Complex Decollement Beneath Nepal

To determine a geometrical model of the MHT at a depth based on our hypocentral locations (Figure 2.4a), we could simply calculate a single best-fitting plane (or line in a two-dimensional model) to our data; however, this would not accurately resolve the indeterminate shape (blob) of seismicity that spans 10–20 km depth from 48–70 km north of the MBT. Therefore, after collapsing our data onto a plane striking N22° E, we divide our catalogue into three parts along-strike: the southern band, the blob that we infer to be a zone of structural complexity labelled 'Duplex' on Figure 2.2a and a northern band (Figure 2.4a). After applying a quantitative procedure based on the southern and northern bands of seismicity (Methods), we determine two fault planes for the MHT that dip ∼2° north-northeast from 15–15.8 km depth and ∼5° north northeast from 17.8–19 km depth, respectively, and strike 292°. Furthermore, the down-dip tip of the shallower plane is ∼2 km vertically above and ∼22 km southsouthwest of the up-dip tip of the deeper plane.

To provide geometrical constraints around the zone of structural complexity, we generate nine new moment tensors (Figure 2.3 and Table 2.1) for small events ($M_w \geq 3.3$) using the wvfgrd96 source inversion program (Herrmann, 2013) and supplement them alongside those relocated from the GCMT catalogue (Dziewonski, Chou, and Woodhouse, 1981) and determined by Bai et al. (2019) (Table 2.2). In total, we use 24 moment tensors within the duplex for this analysis. Despite most of the moment tensors showing thrust faulting and having relative uniformity of strike (17 out of 24), a few smaller-magnitude events show normal and strike-slip behaviour, demonstrating the extent of local structural and/or stress heterogeneities. Although a number of dip-slip events have varying degrees

of obliquity, what they all have in common are nodal planes that dip more or less to the north-northeast. As this observation is consistent with the tectonic kinematics (plate motion) of the region (Ader et al., 2012; Bettinelli et al., 2006), we regard these hinterland-dipping nodal planes as representing the true fault planes. Focusing specifically on the thrust events, we identify two distinct groups of moment tensors on the basis of their hypocentre location and magnitude. The first group consists of 14 events that correspond to steeply dipping thrusts within the seismically complex zone, ranging in angles from 20 to 81°. The average dip angle of this range is 44°. The second group consists of three low-angle thrusts—two of them being the Gorkha and Kodari earthquakes—along the base of the complex zone (the sole thrust of the MHT) and have more shallow dips that range from 6 to 14°. The average dip angle for these events is 10°. When collapsing the entire aftershock sequence onto a single cross-section (Figure 2.4a), the steep structures that the moment tensors imply are not readily apparent; however, by creating multiple, smaller-width cross-sections along-strike, we are able to tease out more coherent images of structures varying in orientation and geometry (Figure 2.4b and Figure 2.3B). Bivariate histograms (density plots) of aftershocks for each cross-section (Figure 2.4c and Figure 2.3C) show steep structures within our complex zone of seismicity; in particular, profile line F–F' shows at least three parallel steep structures. The average dip of these three structures (measured directly from Figure 2.4c) is 45°—consistent with the average dip of steeply dipping thrust moment tensors.

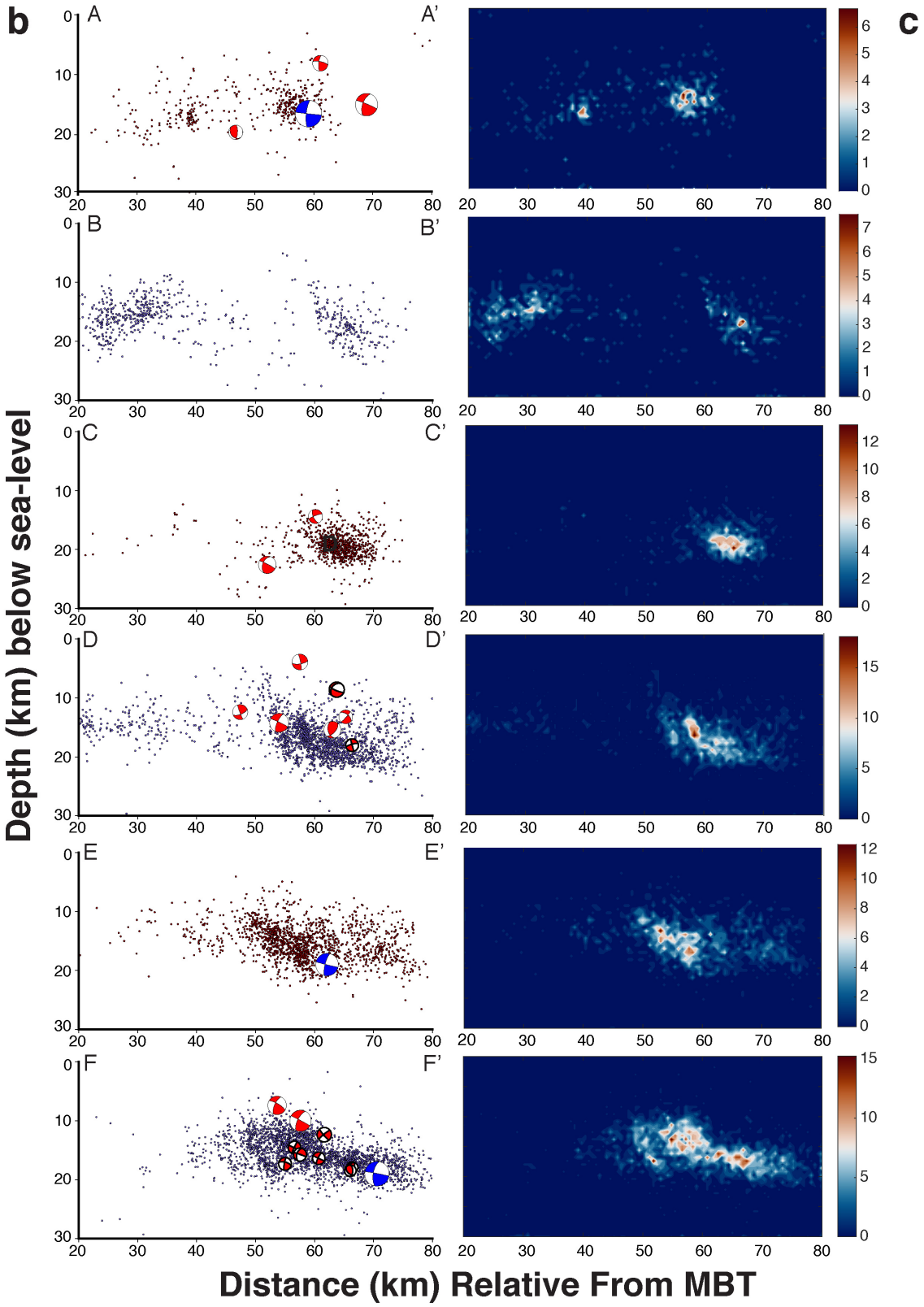
b
c
A
A'
B
B'
C
C'
D
D'
E
E'
F
F'
Depth (km) below sea-level
Distance (km) Relative From MBT

Figure 2.3: Map displaying 6 profile lines equal in length (100 km) and azimuth (22^{o} N), that represent the cross-section profiles in **b**, with westernmost (A–A') on top, easternmost (F–F') on the bottom. We show only moment tensors within the duplex (∼48–70 km) to help constrain structures. **a**, Alternating blue and red stripes of seismicity represent width of seismicity collapsed onto each profile line. **b**, Left-side panels show cross-sections of seismicity. Superimposed in both **a** and **b** are high-quality moment tensor solutions. There are four sets of moment tensors more or less within the duplex: bold are derived from this study, non-bold are from Bai et al. (2019), blue are on the MHT based on their location and large magnitude, and red represent higher-angle faulting struc-tures. **c**, Right-side panels are density plots for each adjacent cross-section of **b**. While the majority of the profiles shown are interpreted to have active steeply dipping structures, the inferred duplex is best observed in the bottommost panels, and in the map at about 86^{o}E longitude. Visually, there are at least three steeply dipping faults at ∼45° between 10 to 20 km depth (profile F–F'). All cross-sections are true-scale. Depths are measured below sea level.

ID	Lon	Lat	Depth (km)	Strike	Dip	Rake	Mag (Mw)	Fit
2015119	85.765	27.884	8.6	268	25	125	4.5	0.6148
2015180	85.779	27.905	18.0	297	75	103	3.8	0.6203
2015205	86.302	27.634	16.4	290	25	95	3.7	0.4914
2015244	86.220	27.611	17.3	355	27	157	3.8	0.6443
2015278	86.152	27.705	12.4	290	50	-90	4.2	0.6924
2015279_12	86.099	27.686	15.7	300	20	-45	3.9	0.6411
2015279_23	86.092	27.680	14.6	285	25	-95	3.8	0.5503
2016015_13	86.235	27.718	17.9	55	75	-10	3.3	0.6350
2016015_17	86.234	27.716	18.5	330	90	-150	3.4	0.6134

Table 2.1: Information for nine high-quality (goodness of fit >50%) moment tensor solutions that are within the duplex. As the moment tensor solution can be sensitive to the location accuracy, we first relocated events by manually picking the P and S-wave arrivals. For each event in the subsequent inversion process we use a minimum of four well-distributed stations. Italicized numbers represent strike-slip events. The non-italicized numbers represent dip-slip events, where we show information for nodal planes that dip more or less NNE (hinterland).

ID	Lon	Lat	Depth (km)	Strike	Dip	Rake	Mag
1	84.766	28.239	16.5	287	6	96	7.8
2	84.859	28.299	15.0	308	23	131	6.6
4	86.014	27.767	19.0	289	14	98	6.7
5	85.817	27.766	14.2	305	26	115	5.6
6	86.130	27.803	19.0	307	11	127	7.3
7	86.207	27.642	10.0	299	28	116	6.3
8	86.200	27,606	7.4	324	34	138	5.5
9	85.596	27.917	14.4	338	82	111	4.2
11	85.750	27.728	12.4	291	70	64	4.5
12	84.915	28.058	19.6	227	72	3	4.2
13	85.727	27.892	15.4	250	80	35	5.0
14	84.780	28.252	8.1	351	21	163	4.6
15	85.495	27.877	22.6	309	28	147	5.2
16	85.720	27.840	3.9	302	79	71	4.7
18	85.720	27.918	13.2	343	49	118	4.1

Table 2.2: Fifteen of eighteen moment tensor solutions determined by Bai et al. (2019). As in Table S1, we only list moment tensor solutions that are within the duplex, strike-slip events are italicized, and for dip-slip events we list the NNE-dipping nodal plane.

2.6 Lesser Himalaya Duplex

Previous workers have suggested that the high microseismic activity beneath the foothills of the Lesser Himalaya occurs on a more-steeply dipping MHT plane (J.-P. Avouac et al., 2015; Elliott et al., 2016; Pandey et al., 1995) —a mid-crustal 'ramp'. Such a ramp linking the down-dip tip of our shallow southern segment of the MHT with the up-dip tip of our deeper northern segment would dip ∼8° and be analogous to this geometry. However, on the basis of moment tensors and earthquake distributions (Figure 2.4b and Figure 2.3B), we interpret the diffuse area of seismicity as a duplex—a series of steeply dipping imbricate faults bounded by a sole and roof thrust. The duplex is most clearly recognized in the easternmost cross-section (Figure 2.4b, profile line F–F'), where at least three high-angle active faults between 10 and 20 km are illuminated by the aftershock

distribution. Robust moment tensors (Figure 2.4b) corroborate activity on these steeply dipping faults. Furthermore, the 2015 M_w 7.3 Kodari earthquake (blue moment tensor, Figure 2.4b) probably indicates the location of the MHT below. Although the increasingly low level of aftershock activity towards the western part of our study area is insufficient to clearly define a similar duplex, this does not necessarily mean that the along-strike extent of the duplex is limited—the low seismic activity may have simply failed to illuminate the duplex there.

Field mapping performed near our study areas in central (Khanal et al., 2015; Subodha Khanal and Robinson, 2013) and western Nepal (Robinson and A. J. Martin, 2014) suggests that seismicity from 5 to 20 km depth is associated with the development of a Lesser Himalayan duplex; coincidently, vertically above this zone of seismicity—to the surface trace of the Main Central Thrust (MCT)—is where the maximum rates of surface uplift and horizontal convergence between India and southern Tibet are measured (Bilham, Larson, and Freymueller, 1997). The development of a duplex system has been inferred to occur by the southward migration of a more localized ramp—in contrast to one that is much larger and shallowly dipping (Elliott et al., 2016; Duputel et al., 2016; Whipple et al., 2016; Cattin and J. Avouac, 2000)—along the MHT, which is the leading edge of the sole thrust of a duplex (Khanal et al., 2015; Robinson and A. J. Martin, 2014), where material is successively scraped off the underthrusting Indian plate. As this ramp propagates southward, more thrust sheets (older ramps) are incorporated into the Lesser Himalaya duplex. This stacking process of similar lithological units tends to express itself at surface-level—before erosional unroofing (present-day outcrops)—by passively folding the overlying crystalline rock and

forming a large foreland-verging thrust-cored antiform (Subodha Khanal and Robinson, 2013). A local example of this is the partly eroded Gorkha–Pokhara antiform (Subodha Khanal and Robinson, 2013) to the western side of our network, between the MCT and Kathmandu Klippe (a remnant thrust-sheet outlier). The MCT in particular is responsible for carrying the Greater Himalayan Kathmandu Klippe 125 km over the Lesser Himalaya, which includes the Ramgarh–Munsiari thrust and the rocks within the duplex (Robinson and McQuarrie, 2012). In central Nepal, a regional antiform is depicted north of Kathmandu, where studies infer that the southward overthrusting/duplexing of younger greenschist-facies metasedimentary rocks of the Lesser Himalayan Sequence began beneath the older MCT (Khanal et al., 2015) during the mid-Miocene (Robinson and McQuarrie, 2012). These surface observations of a duplex in central and western Nepal help us to infer that the intense seismicity between 48–70 km north of the MBT along the entire length of the aftershock zone may illuminate parts of the duplex system with varying levels of activity. Hence, the MHT in this area is not confined to a single ramp/thrust.

Investigations that have employed other methods—for example, thermal and kinematic modelling (Bollinger et al., 2004)—are consistent with the aforementioned geological studies, as they explore the mechanisms behind crustal shortening in this region. Whipple et al. (2016) complement our observations with geodetic (interferometric synthetic aperture radar and GPS) data around the Gorkha and Kodari earthquakes. They suggest that an out-of-sequence steeply dipping fault at the foot of the Greater Himalaya—one that could have initially manifested within a duplex and eventually breached the roof thrust to more shallow depths above the MHT—is mechanically necessary to explain the present-day scenario of in-

ternal deformation that is capable of sustaining topographic uplift. Other geophysics-based studies have argued for a mid-crustal ramp on the MHT, beneath the Greater Himalaya foothills—such as implied between the front and rear of our duplex (Figure 2.4a)—as the primary driver for topographic growth (Elliott et al., 2016; Pandey et al., 1995; Cattin and J. Avouac, 2000). In a similar location to these proposed geometrical models, we observe a duplex, providing a mechanism of internal deformation and consequent high topography along the Himalayan arc (Bollinger et al., 2004; Whipple et al., 2016; Pandey et al., 1995).

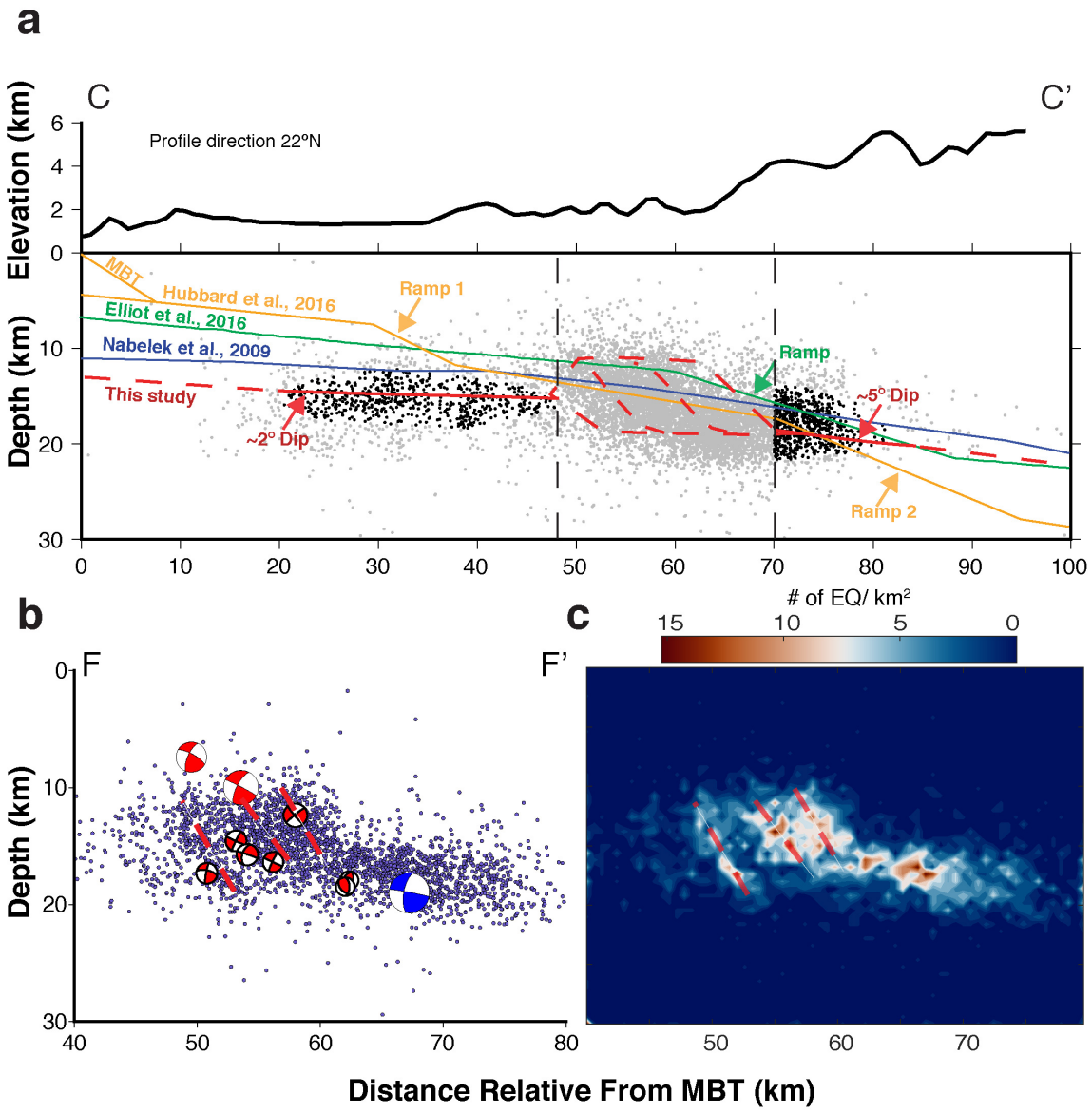
a
C
C'
Profile direction 22°N
Elevation (km)
6
4
2
0
Depth (km)
10
20
30
MBT
Hubbard et al., 2016
Elliot et al., 2016
Nabelek et al., 2009
This study
Ramp 1
Ramp
Ramp 2
~2° Dip
~5° Dip
0
10
20
30
40
50
60
70
80
90
100
b
F
F'
Depth (km)
0
10
20
30
40
50
60
70
80
c
# of EQ/ km²
15
10
5
0
50
60
70
Distance Relative From MBT (km)

Figure 2.4: Topographic and cross-sectional profiles. **a**, All hypocentre events (dots) collapsed onto profile line C–C' (Figure 2.2a), which trends 22° from north at a distance perpendicularly away from the MBT. Solid lines represent models of the MHT along C–C': Hubbard et al. (2016) (orange), Elliott et al. (2016) (green), Nábělek et al. (2009) (blue), and this study (red). Vertical black dashed lines represent northern and southern limits of the 'complex zone' that is removed before contouring. Black dots represent hypocentres used for determining best-fit lines (solid red lines)—that represent our upper and lower MHT plane — after contouring. The grey dots in the middle represent the zone of structural complexity (the duplex). Our interpretation of a continuous MHT—where seismicity is sparse in the southernmost and northernmost ends, and intense within a duplex—is shown as red dashed lines. **b**, Here, the easternmost seismicity is collapsed onto profile line F–F' (Figure 2.2a; events shown in purple), and overlaid by moment tensors using the same colour and line-width scheme as in Figure 2.2a. We note that all red moment tensors indicate steep-angle faulting within the duplex, whereas the more shallowly dipping blue moment tensor (the 2015 Mw 7.3 Kodari earthquake) is inferred to be located on the sole thrust of the MHT. **c**, Density plot of the same zone of seismicity as **b**, but with the purpose of highlighting active fault structures. Both **b** and **c** are annotated with red dashed lines to show inferred imbricate faults within the duplex. There appears to be at least three steeply dipping faults at ∼45° dip between 10 and 20 km depths. These structures are best observed within a cross-section 35 km wide at 86° E. All cross-sections are true scale and plotted below mean sea level.

2.7 Reconciling Previous Models

In the model proposed here for the MHT in Nepal, the southern, shallower plane is well constrained by 587 events spanning ∼30 km down-dip. The northern, deeper plane is less constrained since events dramatically decrease in abundance as they span ∼15 km down-dip. The duplex in the zone of seismic complexity is the cardinal feature that connects these two planes. In Figure 2.4a, we compare our duplex model—which is based on our high-resolution seismicity catalogue and moment tensors—with a select group of previous models that effectively highlight the most common geometric interpretations of the MHT in the same general area. On the basis of geology and source parameters of the Gorkha earthquake, Hubbard et al. (2016) developed a model that shows the MHT as having a middle ramp and a deep ramp that dip at 26°, and are separated by a middle (flat) décollement shallowly dipping at 7°. North of the deep ramp, the décollement flattens out again, dipping at 7°. Our proposed duplex lies between the two ramps proposed by Hubbard et al. (2016). From geodetic data, Elliott et al. (2016) suggest that the MHT has a single, steep 15–25° mid-crustal ramp in the region of our duplex, connecting two flat segments (5° and 5–7°). Although our model has similar flat segments to theirs, ours involves a complex duplex as opposed to a single mid-crustal ramp. This difference should be expected, though, since geodetic models lack the resolution to distinguish between a duplex and a single ramp at this depth. By contrast, receiver function images from the Hi-CLIMB (Himalayan-Tibetan Continental Lithosphere During Mountain Building) experiment (Nábělek et al., 2009) show a small but continuous increase in the dip of the MHT that begins beneath the Greater Himalaya, as opposed to having either a flat ramp–flat geometry or a duplex. In contrast

to these previous models that have lower spatial resolution (Elliott et al., 2016; Nábělek et al., 2009) or rely on assumptions about fault geometries (Hubbard et al., 2016), our model is derived directly from earthquake activity on the faults we seek to image, so it is inherently more likely to capture the true complexity of the MHT. The other notable difference in our model is that our southern flat segment, well constrained by the copious aftershock seismicity and within the likely uncertainty of the previous receiver–function image (Nábělek et al., 2009), is substantially deeper beneath the Kathmandu Klippe than a model based only on the main shock (Elliott et al., 2016) plus assumptions about possible geological constraints (Hubbard et al., 2016). Because our data contains no evidence for an active 'ramp 1' (Figure 2.4a), our model has a much larger cross-sectional accommodation area above the active MHT that will require redrawing of existing balanced cross-sections.

2.8 Conclusions

In conclusion, we present a new model of the MHT in Nepal based on the M_w 7.8 Gorkha earthquake aftershock sequence that occurred primarily along the locked-to-creeping transition within a duplex. In doing so we reconcile surface geological observations (Khanal et al., 2015; Robinson and A. J. Martin, 2014; DeCelles et al., 2001; Hubbard et al., 2016; Wobus et al., 2005; Bollinger et al., 2004) with geophysical studies (Elliott et al., 2016; Duputel et al., 2016; Whipple et al., 2016; Gao et al., 2016; Nábělek et al., 2009; Lemonnier et al., 1999) surrounding complex structural characteristics of the MHT, as it has critical implications for Himalayan tectonics, kinematic models, earthquake source dynamics and seismic hazard. Tectonic stress is accommodated by an actively deforming

duplex, particularly by the steeply dipping imbricate faults within it. The geometrical transition of the MHT from planar, to duplex, to planar again probably acts as an internally deforming tectonic doorstop that essentially impedes subduction of the Indian plate, causing stress concentrations on highly sensitive faults (Mendoza, Ghosh, and Rai, 2016) that may help nucleate and control the rupture process of large earthquakes along the MHT, such as the 2015 Gorkha event. The presence of this duplex with abrupt and complex changes in dip angles along the MHT is a characteristic of crustal shortening that creates the physiographic transition from Lesser Himalaya into Greater Himalaya (Elliott et al., 2016; Wobus et al., 2005; Pandey et al., 1995; Cattin and J. Avouac, 2000).

Bibliography

Ader, Thomas et al. (2012). "Convergence rate across the Nepal Himalaya and interseismic coupling on the Main Himalayan Thrust: Implications for seismic hazard". In: *Journal of Geophysical Research: Solid Earth* 117.B4.

Adhikari, LB et al. (2015). "The aftershock sequence of the 2015 April 25 Gorkha–Nepal earthquake". In: *Geophysical Supplements to the Monthly Notices of the Royal Astronomical Society* 203.3, pp. 2119–2124.

Ambraseys, NN and J Douglas (2004). "Magnitude calibration of north Indian earthquakes". In: *Geophysical Journal International* 159.1, pp. 165–206.

Avouac, Jean-Philippe et al. (2015). "Lower edge of locked Main Himalayan Thrust unzipped by the 2015 Gorkha earthquake". In: *Nature Geoscience* 8.9, pp. 708–711.

Bai, Ling et al. (2019). "Lateral variation of the Main Himalayan Thrust controls the rupture length of the 2015 Gorkha earthquake in Nepal". In: *Science advances* 5.6, eaav0723.

Bettinelli, Pierre et al. (2006). "Plate motion of India and interseismic strain in the Nepal Himalaya from GPS and DORIS measurements". In: *Journal of Geodesy* 80.8-11, pp. 567–589.

Bilham, Roger (1995). "Location and magnitude of the 1833 Nepal earthquake and its relation to the rupture zones of contiguous great Himalayan earthquakes". In: *Current Science* 69.2, pp. 101–128.

Bilham, Roger (2015). "Raising Kathmandu". In: *Nature Geoscience* 8.8, pp. 582–584.

Bilham, Roger (2019). "Himalayan earthquakes: a review of historical seismicity and early 21st century slip potential". In: *Geological Society, London, Special Publications* 483.1, pp. 423–482.

Bilham, Roger, Vinod K Gaur, and Peter Molnar (2001). "Himalayan seismic hazard". In: *Science* 293.5534, pp. 1442–1444.

Bilham, Roger, Kristine Larson, and Jeffrey Freymueller (1997). "GPS measurements of present-day convergence across the Nepal Himalaya". In: *Nature* 386.6620, pp. 61–64.

Bollinger, Laurent et al. (2004). "Thermal structure and exhumation history of the Lesser Himalaya in central Nepal". In: *Tectonics* 23.5.

Cattin, R and JP Avouac (2000). "Modeling mountain building and the seismic cycle in the Himalaya of Nepal". In: *Journal of Geophysical Research: Solid Earth* 105.B6, pp. 13389–13407.

Chen, Wang-Ping and Peter Molnar (1977). "Seismic moments of major earthquakes and the average rate of slip in central Asia". In: *Journal of Geophysical Research* 82.20, pp. 2945–2969.

Dal Zilio, Luca et al. (2019). "Bimodal seismicity in the Himalaya controlled by fault friction and geometry". In: *Nature communications* 10.1, pp. 1–11.

DeCelles, Peter G et al. (2001). "Stratigraphy, structure, and tectonic evolution of the Himalayan fold-thrust belt in western Nepal". In: *Tectonics* 20.4, pp. 487–509.

Duputel, Zacharie et al. (2016). "The 2015 Gorkha earthquake: a large event illuminating the Main Himalayan Thrust fault". In: *Geophysical Research Letters* 43.6, pp. 2517–2525.

Dziewonski, AM, T-A Chou, and John H Woodhouse (1981). "Determination of earthquake source parameters from waveform data for studies of global and regional seismicity". In: *Journal of Geophysical Research: Solid Earth* 86.B4, pp. 2825–2852.

Elliott, JR et al. (2016). "Himalayan megathrust geometry and relation to topography revealed by the Gorkha earthquake". In: *Nature Geoscience* 9.2, pp. 174–180.

Gao, Rui et al. (2016). "Crustal-scale duplexing beneath the Yarlung Zangbo suture in the western Himalaya". In: *Nature Geoscience* 9.7, pp. 555–560.

Grandin, Raphaël et al. (2015). "Rupture process of the Mw= 7.9 2015 Gorkha earthquake (Nepal): Insights into Himalayan megathrust segmentation". In: *Geophysical Research Letters* 42.20, pp. 8373–8382.

Gualandi, Adriano et al. (2017). "Pre-and post-seismic deformation related to the 2015, Mw7. 8 Gorkha earthquake, Nepal". In: *Tectonophysics* 714, pp. 90–106.

Herrmann, Robert B (2013). "Computer programs in seismology: An evolving tool for instruction and research". In: *Seismological Research Letters* 84.6, pp. 1081–1088.

Hubbard, Judith et al. (2016). "Structural segmentation controlled the 2015 Mw 7.8 Gorkha earthquake rupture in Nepal". In: *Geology* 44.8, pp. 639–642.

Karplus, Marianne S et al. (2015). "Aftershocks of the M7. 8 Gorkha (Nepal) earthquake: Early results from project NAMASTE". In: *AGU Fall Meeting Abstracts*. Vol. 2015, S41D–07.

Khanal, S et al. (2015). "Evidence for a far-traveled thrust sheet in the Greater Himalayan thrust system, and an alternative model to building the Himalaya". In: *Tectonics* 34.1, pp. 31–52.

Khanal, Subodha and Delores M Robinson (2013). "Upper crustal shortening and forward modeling of the Himalayan thrust belt along the Budhi-Gandaki River, central Nepal". In: *International Journal of Earth Sciences* 102.7, pp. 1871–1891.

Lemonnier, Carole et al. (1999). "Electrical structure of the Himalaya of central Nepal: High conductivity around the mid-crustal ramp along the MHT". In: *Geophysical Research Letters* 26.21, pp. 3261–3264.

Martin, Stacey S, Susan E Hough, and Charleen Hung (2015). "Ground motions from the 2015 M w 7.8 Gorkha, Nepal, earthquake constrained by a detailed assessment of macroseismic data". In: *Seismological Research Letters* 86.6, pp. 1524–1532.

Mendoza, Manuel M, Abhijit Ghosh, and Shyam S Rai (2016). "Dynamic triggering of small local earthquakes in the central Himalaya". In: *Geophysical Research Letters* 43.18, pp. 9581–9587.

Mugnier, Jean-Louis et al. (2017). "Segmentation of the Himalayan megathrust around the Gorkha earthquake (25 April 2015) in Nepal". In: *Journal of Asian Earth Sciences* 141, pp. 236–252.

Nábělek, John et al. (2009). "Underplating in the Himalaya-Tibet collision zone revealed by the Hi-CLIMB experiment". In: *Science* 325.5946, pp. 1371–1374.

Paige, Christopher C and Michael A Saunders (1982). "LSQR: An algorithm for sparse linear equations and sparse least squares". In: *ACM Transactions on Mathematical Software (TOMS)* 8.1, pp. 43–71.

Pandey, MR et al. (1995). "Interseismic strain accumulation on the Himalayan crustal ramp (Nepal)". In: *Geophysical Research Letters* 22.7, pp. 751–754.

Robinson, Delores M and Aaron J Martin (2014). "Reconstructing the Greater Indian margin: A balanced cross section in central Nepal focusing on the Lesser Himalayan duplex". In: *Tectonics* 33.11, pp. 2143–2168.

Robinson, Delores M and Nadine McQuarrie (2012). "Pulsed deformation and variable slip rates within the central Himalayan thrust belt". In: *Lithosphere* 4.5, pp. 449–464.

Ross, ZE et al. (2016). "An improved algorithm for real-time S-wave picking with application to the (augmented) ANZA network in Southern California". In: *Bulletin of the Seismological Society of America* 106.5, pp. 2013–2022.

Sapkota, SN et al. (2013). "Primary surface ruptures of the great Himalayan earthquakes in 1934 and 1255". In: *Nature Geoscience* 6.1, pp. 71–76.

Waldhauser, Felix and William L Ellsworth (2000). "A double-difference earthquake location algorithm: Method and application to the northern Hayward fault, California". In: *Bulletin of the Seismological Society of America* 90.6, pp. 1353–1368.

Whipple, Kelin X et al. (2016). "Active shortening within the Himalayan orogenic wedge implied by the 2015 Gorkha earthquake". In: *Nature Geoscience* 9.9, pp. 711–716.

Wiemer, Stefan (2001). "A software package to analyze seismicity: ZMAP". In: *Seismological Research Letters* 72.3, pp. 373–382.

Wobus, Cameron et al. (2005). "Active out-of-sequence thrust faulting in the central Nepalese Himalaya". In: *Nature* 434.7036, pp. 1008–1011.

Chapter 3

Duplex and Moho Earthquakes Beneath the Lesser Himalaya in India

3.1 Abstract

In this study we investigate small earthquakes occurring in the crust and lithospheric mantle beneath the Indian state of Uttarakhand. This region resides at the westernmost end of what is referred to as the 'central seismic gap', where a great ($\geq$M8) plate boundary earthquake has not occurred along the Main Himalayan Thrust (MHT) in over 500 years. While the up-dip portion of the MHT remains frictionally locked, background seismicity observed down to near-Moho depths provides insight into how the Himalayas arc is actively deforming and contributing to the genesis of future large earthquakes. In the up-

per crust (<25 km), a dense band of NW-SE trending seismicity indicates active structures immediately south of the physiographic transition from the Lesser to Higher Himalaya. Most notably, a dense cluster of earthquakes in proximity to the 1999 Mw 6.5 Chamoli earthquake delineate two moderately dipping faults splaying above the MHT. With the addition of focal mechanisms, we infer these faults to be imbricate and associated with a Lesser Himalaya duplex. Such a structure is consistent with surface geological interpretations and seismological observations made elsewhere along the arc, suggesting it may play a significant role in accommodating plate convergence between the Indian and Eurasian plate. In the lower crust and lithospheric mantle (30-60 km)—where it is argued that conditions are unfavorable for brittle failure to occur—we provide evidence for the existence of earthquakes. Most focal mechanisms for select high-quality earthquakes indicate normal faulting. We infer such seismicity at near-Moho depths beneath the Lesser Himalaya to reflect flexural bending of the Indian lithosphere. This observation challenges the notion that the strength of the lithosphere is confined to the crust, and suggests that dynamic processes (such as underplating) are promoting brittle deformation deep beneath the Himalayas.

3.2 Introduction

The distribution and source characteristics of micro-to-moderate sized earthquakes provide important insight into our understanding of tectonic processes controlling deformation along major plate boundaries and the larger devastating earthquakes they host. In the case of the Himalayas, a 2,400 km-long continental collision zone supporting the tallest mountains in the world, it is widely observed that the bulk of near-incessant seismic activ-

ity occurs at shallow depths along subsidiary fault structures manifesting above the plate boundary, the Main Himalayan Thrust (MHT) (e.g., Arora et al., 2007; N. Kumar, Paul, et al., 2012; A. F. Sheehan et al., 2008; Negi et al., 2017; Ni and Barazangi, 1984). On the other hand, the generation of strong to great plate boundary-type earthquakes are usually confined to the MHT itself over centennial to millennial timescales (e.g., Bilham, 2019; C. Rajendran and K. Rajendran, 2005; Mugnier et al., 2013; Dal Zilio et al., 2019; Stevens and Avouac, 2016; Vorobieva, Mandal, and Gorshkov, 2017). The most recent major earthquake to have violently slipped a segment of the MHT, the 2015 Mw 7.8 Gorkha earthquake in central Nepal, produced thousands of aftershocks along its lower locked interface and in the thrust hanging wall. This provided a rare opportunity immediately during the post-seismic period to sample new information on the dynamics of the MHT and overall tectonics of the Himalayas (e.g., M. Mendoza et al., 2019; Baillard et al., 2017; Adhikari et al., 2021; Karplus et al., 2020; Gualandi et al., 2017; Elliott et al., 2016; Bai et al., 2019). Moreover, there has been renewed concern about the general timing and location of such large events that are likely to occur immediately beyond the Gorkha rupture area, or elsewhere along the arc. Thus, knowledge gained from the Gorkha earthquake should be applied to other segments of the MHT currently stockpiling enough strain capable of producing the next large earthquake. In this study, we turn our attention to the Indian state of Uttarakhand, which resides in a segment of the MHT at the western end of what is known as the ‘central seismic gap. This gap is inferred to not have hosted a great earthquake in over 500 years (Bilham, 2019; H. Srivastava et al., 2015; Prasath, Paul, and S. Singh, 2019)—others argue that it has been over a millennium (e.g., C. Rajendran and K. Rajendran, 2005). Unlike the

Gorkha segment, this gap is late in its earthquake cycle and experiencing a seismic lull of mostly small-magnitude earthquakes. We use these earthquakes to characterize lithospheric scale pre-seismic deformation taking place in Uttarakhand to further our understanding of Himalayan seismotectonics and seismogenesis. Since the 1980's seismic experiments in this region have observed an active and dense NNW-SSE band of seismicity that trends adjacent to (but not on) the Main Central Thrust (MCT) zone, which demarcates the physiographic transition of the Lesser to Higher Himalaya (Kayal et al., 2003; Negi et al., 2017; Seeber and Armbruster, 1984; Ni and Barazangi, 1984; Prasath, Paul, and S. Singh, 2019). In Uttarakhand, the MCT zone consists of old high-grade metamorphic rock sandwiched between the presently dormant Munsiari (MCT-I) and Vaikrita (MCT-II) Thrusts that splay off the down-dip extent of the MHT. Other characteristic major Himalayan fault structures include the surface-breaching Main Boundary Thrust (MBT) and Main Frontal Thrust (MFT) to the south. They are inferred to break during great earthquakes via southward rupture propagation along the up-dip locked portion of the MHT (Bilham, 2019; Bollinger et al., 2014; S. Kumar et al., 2001). Situated be-tween the MBT and MCT zone, deformation in the Lesser Himalaya consists of metasedimentary rocks that are actively folding and faulting, forming the bulk of the Himalaya accretionary wedge. It is here in this seismically active area where crustal shortening accommodates a significant portion of Indian and Eurasian plate convergence occurring at an average rate of 15 mm/yr (Bilham, 2019). Many geological and geophysical studies have set out to delineate the fault architecture of the Lesser Himalaya to understand its role in supporting the Himalayas and controlling the rupture process of large Himalayan earthquakes. Still, subsurface interpretations from geological

observations are limited by assumptions derived at the surface; while geophysical methods face the challenge of imaging/mapping the subsurface in sufficient resolution to discern finer scale structural features. At depths below the MHT, recent studies in Uttarakhand have also observed sparse and indeterminate seismicity occurring near the Mohorovicic Discontinuity (Moho) and associate it with flexure of the Indian plate as it underthrusts southern Tibet (Ni and Barazangi, 1984; Mahesh, S. Gupta, et al., 2015; Lyon-Caen and Molnar, 1983). However, those studies expended little focus into earthquakes occur-ring at those depths beneath the Himalayas; an important observation where it is argued that the lithosphere is incapable of yielding brittle failure (e.g., Jackson, 2002). We address these issues using waveform data from a local seismic network in Uttarakhand to generate a high-resolution earthquake catalog. From this, we construct an updated model of the MHT by synthesizing results from previous works, and develop a more holistic description on crustal/sub-crustal deformation occurring in this segment of the Himalaya.

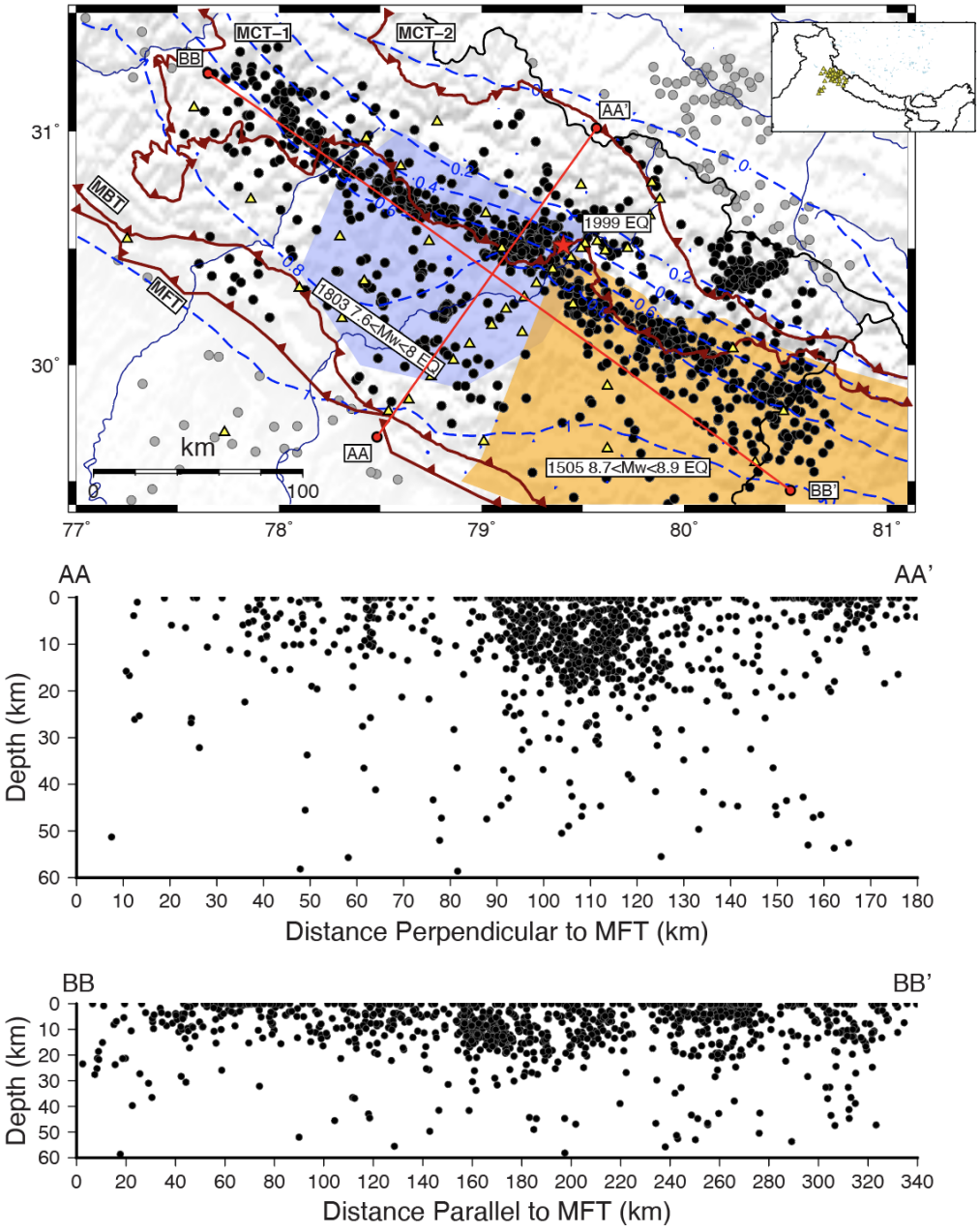
MCT–1
MCT–2
BB
AA'
MBT
MFT
1999 EQ
1803 7.6<Mw<8 EQ
1505 8.7<Mw<8.9 EQ
AA
BB'
km
0
100
31˚
30˚
77˚
78˚
79˚
80˚
81˚
AA
AA'
Depth (km)
Distance Perpendicular to MFT (km)
BB
BB'
Depth (km)
Distance Parallel to MFT (km)

Figure 3.1: Absolute earthquakes locations in Uttarakhand based on waveform data obtained from (Mahesh, S. Rai, et al., 2013). (Top) Network (yellow triangles) map showing a band of seismicity trending NW-SE and adjacent to the surface trace of the MCT-I. Seismicity is sparse to the southwest where the coupling pattern (blue dashed lines; Ader et al., 2012) indicates the up-dip portion of the MHT is strongly locked. Yellow and blue shaded polygons represent the estimated rupture areas of two large historic earthquakes in this region of the Himalaya. The red star shows the USGS location of the 1999 Chamoli earthquake. Earthquakes that are more or less within the bounds of the network (black dots) were projected onto vertical planes (shown in map view as red lines) to create cross-sectional profiles—one perpendicular (35°) and the other parallel (125°) to the approximate strike of the MHT in this area. In these cross-sections, generally, we observe a dense cluster of seismicity above 25 km depth, and a sparse, nonuniform distribution of seismicity below—two main features explored in detail in this study.

3.3 Seismological Network and Methods

Earlier earthquake studies in Uttarakhand relied on the observations of moderate to large earthquakes recorded at regional and teleseismic distances. In 1984, the Wadia Institute of Himalaya Geology (WIHG) added stations to the region; however, they were sparsely distributed and led to an earthquake catalog with magnitude of completeness only down to M $\geq$ 3.8 (N. Kumar, Sharma, et al., 2009). Hence, for some time the limited sensitivity to earthquakes at lower magnitudes resulted in an unclear picture of subsurface structures. In 2005, WIHG and CSIR upgraded Uttarakhand's seismic network, making it possible to capture a wider range of earthquake magnitudes in the region, and with greater accuracy on hypocenter locations. This network operated from 2005 to 2008 and consisted of 50 digital broadband stations that stretched from the Ganga basin to the Higher Himalaya (Figure 3.1)—more details about this network can be found in Mahesh, S. Rai, et al. (2013). The procedures detailed in this study use waveform data from this network. Specifically, we use 20 months of data from October 2006 to June 2008, since this is when the network was laterally distributed along the Sub and Lesser-Himalaya and could provide more robust location estimates.

Earthquake detection and phase association. For decades the development of earthquake catalogs have used techniques such as the short-time average/long-time average (STA/LTA) ratio algorithm, to automatically detect ("pick") characteristics earthquake phase arrivals in the waveform record. However, as encountered in the preliminary stages of this study, even with carefully fine-tuned parameterization this technique fails to identify many earthquakes occurring locally; and instead, often picked non-earthquake signals or

earthquakes that occurred at distances well-outside the network. These early missteps in the detection stage can lead to P and S-phase misidentification and consequently bad location estimates, requiring laborious "cleaning-up" or post-processing of the catalog. To help combat this problem, we use an attentive deep-learning model from the python software package EQTransformer (Mousavi et al., 2020). This artificial intelligence-based approach simultaneously detects earthquakes signals in continuous waveform data and picks P and S phases. These two actions working in tandem have proven to significantly minimize the number of false negative and false positive signal detection rates, improving the temporal accuracy of arrival times picks, and leading to more reliable location estimates. The model developed by Mousavi et al. (2020) was trained using 1 M earthquakes from a variety of tectonic environments across the world; except in Japan, where it was able to detect double the number of aftershocks produced by the 2000 Mw 6.6 Tottori earthquake (Fukuyama et al., 2003). This indicated the high generalization and accuracy of the model, and is the reason why we employ it here. Further, the user-end application of EQTransformer is straight-forward and requires fewer parameter tuning than using the STA/LTA method. In this study, the model was used in batch mode on the Uttarakhand waveform dataset, and causally band-passed at 1-12 Hz. Earthquakes were detected using a prediction probability threshold of 0.3, whereas the threshold for picking P and S-phases were set to 0.1 for each – default parameter values that detected more local events in the waveform data compared to the STA/LTA algorithm used in Antelope (BRTT). Given the objectives of this study, we found EQTransformer to be very effective in detecting local seismicity, as opposed to our earlier STA/LTA-based detections, which had contaminated our earlier, preliminary

catalog with regional and teleseismic events. This is an unsurprising consequence given the networks placement in a highly active and large tectonic regime. The efficacy in detecting less events beyond the aperture of the network is likely owed to the AI model having been trained on seismic stations recording event epicentral distances no greater than 300 km.

Absolute earthquake catalog. EQTransformer detections and phase picks were then imported into Antelope (BRTT) to be associated with a preliminary event location on a 3-D travel-time grid using a local 1-D velocity model (Mahesh, S. Rai, et al., 2013). To better constrain those earthquakes occurring at greater depths, we combine the Mahesh, S. Rai, et al. (2013) velocity model with an additional velocity layer obtained by Negi et al. (2017), who used the travel-time distance curve method to delineate the Moho at 46 km in Uttarakhand. Next, we further refine locations by relocating the events using the generalized earthquake-location (GENLOC) inversion program (Pavlis et al., 2004) in Antelope (BRTT). Events that were not located by at least 5 stations were discarded, as well as those events that were located outside the aperture of the network. Local magnitudes are then computed on relocated events using Antelopes 'dbevproc' local magnitude calculator. To help ensure that our catalog contained earthquakes well-constrained at depth, we discarded those that were located with no S-phases—i.e., all earthquakes in our catalog have at least one S-phase used in the location procedure. The combined detection, phase association, and location procedures described here yield an earthquake catalog containing 1,213 events. Error statistics for this catalog are shown in the Supplementary Materials (Figure 3.2).

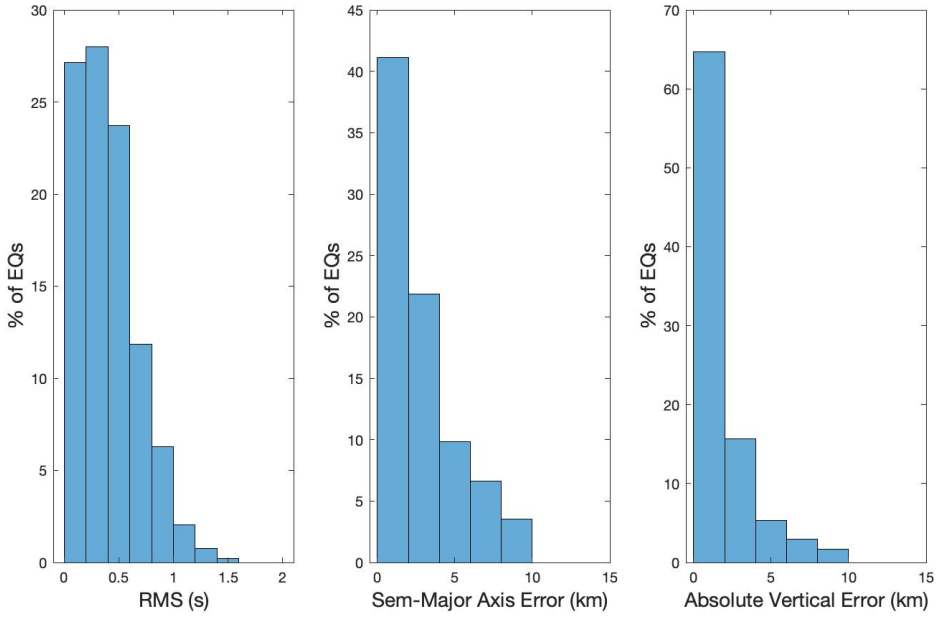

Figure 3.2: Histogram showing error statistics for travel time residuals (s), largest horizontal error (km), and vertical/depth error (km).

Relocated earthquake catalog. To better delimit the locations of fault structures and their geometries, we once again relocated events using the same velocity model described above, but this time by passing events from our absolute (Antelope) catalog into HypoDD (Waldhauser and Ellsworth, 2000). Catalog travel-time phase picks and waveform cross-correlation differential times are used to relocate events using the conjugate gradients method (LSQR) (Paige and Saunders, 1982) in HypoDD. Regarding some of the important criteria used for relocation: P-phases were assigned a weight of 1.0, while S-phases were assigned a smaller weight of 0.5 (due to their relatively lower signal to noise ratio); events had to have at least 5 phase arrivals; and were a maximum of 10 km away from their nearest neighboring event. As a result of this parameter setup, many outlying events and those that

got shifted above sea level (as "airquakes") by consequence of the iteration process, were discarded. This resulted in a second, more tightly clustered catalog containing 736 events.

Computing focal mechanisms. To determine orientations and deformation styles of fault structures, we obtained focal mechanisms based on P-wave first-motion polarities using the HASH software (Hardebeck and Shearer, 2008). A minimum of 8 P-wave polarities were manually picked at their onset times to compute the 'preferred' (and auxiliary) fault plane solution for each earth-quake. The few ambiguous P-wave signals whose polarities appeared more emergent/less-impulsive within the background noise were assigned a lower weight. We employ the same 1-D velocity model used in the location procedure to perturb source depth, compute take-off angles, and determine the best focal mechanism solutions with uncertainty estimates. Following the quality criteria developed by Hardebeck and Shearer (2008), we use only focal mechanisms with a quality of C or better, which equates to a 70% or greater probability at which the real (true) mechanism is "close" to the preferred (computed) mechanism.

3.4 Results

In Figure 3.1, we show the distribution of 1,314 earthquakes in Uttarakhand resulting from the EQTransformer and Antelope procedures, plotted with interseismic coupling lines along the MHT (Ader et al., 2012) and estimated rupture areas of two historic earthquakes in the region. In map view, we observe a dense NW-SE band of seismicity trending sub-parallel to the MCT-1, at the foot of the physiographic transition from the Lesser to Higher Himalaya and mostly along an area of intermediate coupling (0.6). There are two

very shallow clusters of seismicity to the northeast and just beyond the MCT-II. Since these clusters reside outside the aperture of the network, their hypocentral locations are likely poorly constrained and therefore not examined in this study. Towards the MFT in the southwest, seismicity is sparse, indicating that little deformation is taking place; or if so, it is probably occurring aseismically. This comes as no surprise since the coupling pattern indicates that the MHT and its surface breaching thrusts are frictionally locked here. To gain a first order understanding of the distribution of seismicity at depth, we refer to the two cross-sectional profiles shown in Figure 3.1. From these perspectives, we observe two important features that are the focus of this study: (1) prolific seismicity clustered above 25 km depth directly below the surface trace of the MCT-I; and (2) earthquakes near the lower crust and upper mantle boundary.

Next, we turn to our high resolution HypoDD catalog to examine the band of NW-SE trending seismicity more carefully along the MHT. In Figure 2, a second map shows a thinner band of seismicity along with the locations of six arc-perpendicular depth profiles used to carefully examine any along-strike structural variation. To help delineate the spatial extent and orientation of fault structures giving rise to this tight band of seismicity, we supplement a few cross-sections with select focal mechanisms obtained by Mahesh, S. Gupta, et al. (2015). While it is difficult to confidently identify fault structures among the majority of cross-sections, the most coherent and interesting structures that we observe – which we will analyze in greater detail below—reside in Profile C. In this profile we infer two moderately dipping fault planes with dips of 42° and 47°, respectively with increasing distance from the MFT. Additionally, 10 of 11 focal mechanisms indicate thrust faults

striking parallel to the MHT and ranging in dip (for hinterland-directed nodal planes) from 32° to 50°.

Beneath the Lesser Himalaya is the appearance of sparsely distributed seismicity near the Moho (40-60 km). Since it is uncommon to observe brittle deformation taking place at such depths beneath the Himalayan arc, we focus only on the highest quality events before making our interpretations. From our absolute catalog we extract a subset of 10 carefully examined earthquakes that: (1) had the accuracy of their first arrival phase picks visually verified; (2) were located with an azimuthal gap less than 180°; and (3) each had a vertical uncertainty less than 3 km. From this we contend that these deeper events are real, accurate, and at least partially representative of those other unverified deep events shown in cross-section. Of these ten earthquakes, three were also documented by Mahesh, S. Rai, et al. (2013). In that study the authors assessed the events' depth reliability by performing a series of relocation inversions where depth was held fixed at varying intervals, to determine the depth at which the RMS (the standard deviation of the residuals) is at a minimum. Those three earthquakes were found to be occurring at 40-45 km depths in the lower crust. We go a step further and obtain focal mechanisms for those three independently verified near-Moho earthquakes, and the seven more determined from our catalog. Overall, we obtain five normal faulting type focal mechanisms, with the remaining being (three) thrust and (two) strike-slip type.

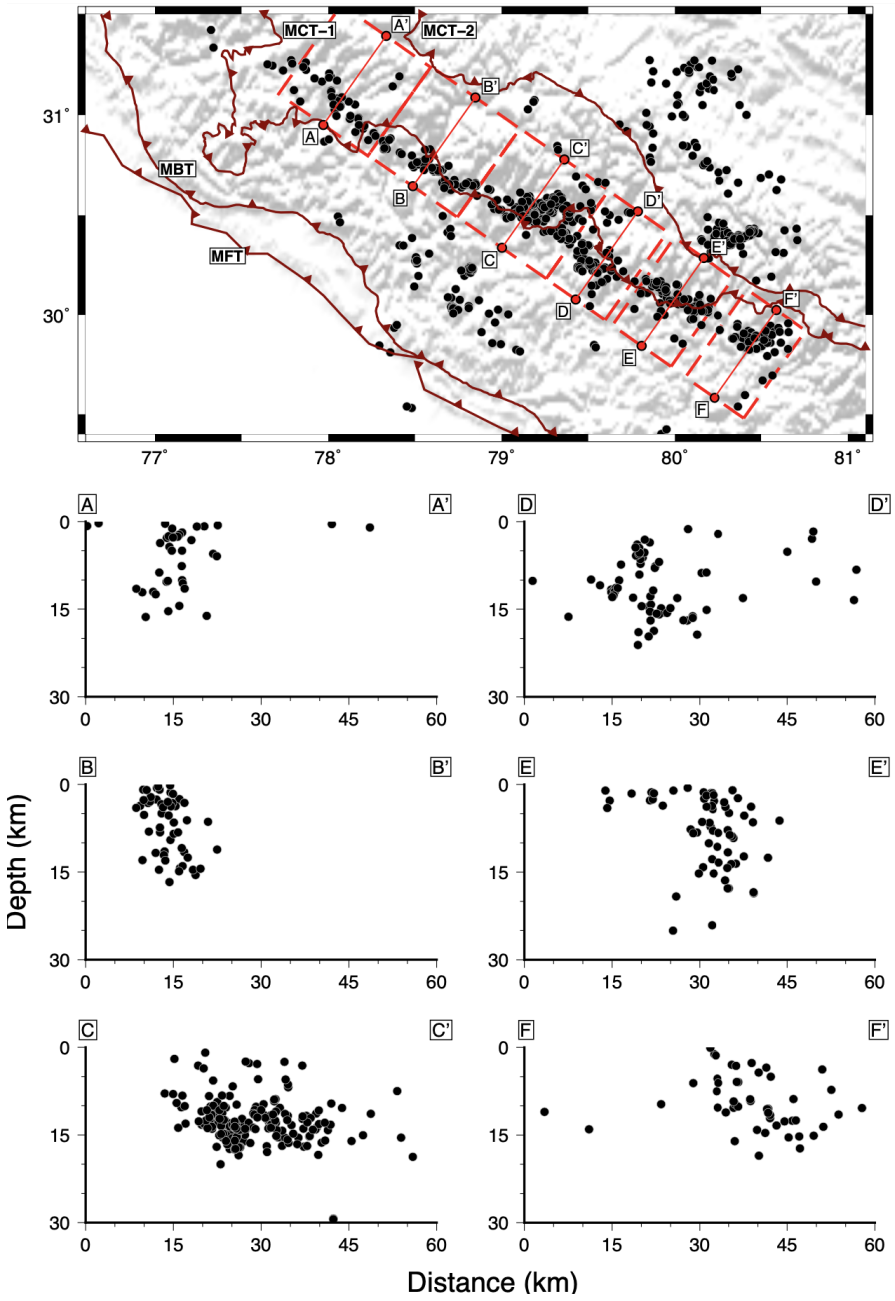

Figure 3.3: HypoDD earthquake locations used to delineate along-strike variation of active fault structures in the Lesser Himalaya. The map shows a tighter cluster of seismicity compared to those shown in Figure 3.1. Additionally, we shown the locations and spatial extent of six profile lines where cross-sections were made. Each of them are roughly the same distance away from the MFT and approx-imately perpendicular to its strike. It is difficult to discern convincingly clear fault structures among most of the cross-sections, especially for those that contain earthquakes located towards the edge of the network. However, where seismic activity is highest near the epicenter of the 1999 Chamoli earthquake (Figure 3.1), we believe that profile C shows the clearest indication of two moderately dipping fault planes above the MHT.

3.5 Lesser Himalayan Duplex in Uttarakhand

Where seismicity is sparse and/or not well-constrained, it is generally difficult to discern coherent structures mapped by seismicity along most of the Lesser Himalaya. In profile C of Figure 3.3, however, we believe to have identified the presence of moderately dipping highly active fault structures in the middle of the seismic network and near the location of the 1999 M 6.5 Chamoli Earthquake. Naturally this brings into question if there is a relationship of some kind. Various studies have postulated that the Chamoli earthquake did not take place on the down-dip sub-horizontal ("flat") portion of the MHT, mainly because its dip indicates that it occurred on a steeper dipping fault surface in the range of 7-15° (K. Rajendran, Parameswaran, and C. Rajendran, 2018; Satyabala and Bilham, 2006; Xu, Bürgmann, and Z. Li, 2016). This has led to some speculation about whether the Chamoli earthquake occurred on an MHT ramp, or on splay faults above it. The general agreement between those studies is that, like the 1991 Mw 6.7 Uttarakashi earthquake to the west, the Chamoli earthquake occurred on a thrust rooting into the down-dip lower plane of the MHT. Since the Chamoli earthquake, our catalog and others show an ongoing and heightened level of seismicity in the hanging wall above its hypocenter. This likely explains why profile C shows the clearest evidence of fault structures within the band of seismicity occurring adjacent to the surface trace of the MCT. Specifically, we discern two moderately dipping thrust faults. Directly from profile C of Figure 3.3, we calculate the southernmost (left) structure to dip at 42°, and the northernmost (right) structure to dip at 47°. Moreover, focal mechanisms obtained by Mahesh, S. Gupta, et al. (2015) for the same events found in our catalog for this area indicate these structures to be predominantly

thrust faults with an average dip of ∼38°. To the west, Negi et al. (2017) obtained a thrust type focal mechanism gently dipping toward the hinterland (Figure 3; no.1) and interpreted it to belong to the Tons Thrust. When projecting this focal mechanism ∼90 km onto profile line C, it is situated directly above the two moderately dipping thrusts observed in this study. Given this evidence, we infer these two active imbricate thrusts to be active components of a Lesser Himalayan Duplex—with the Tons Thrust directly above acting as a sub-horizontal roof—that had either been activated or reactivated in response to the 1999 Chamoli earthquake below near the sole thrust.

For decades geologists have primarily relied on surficial structural geometries along the Himalayan orogenic belt to probe the depth to, development and topography of, the MHT and the subsidiary faults that root into it (e.g., Schelling and Arita, 1991; Saklani, Nainwal, and V. Singh, 1991; Macfarlane, Hodges, and Lux, 1992; P. Srivastava and Mitra, 1994; P. DeCelles et al., 1998; Robinson, Peter G DeCelles, and Copeland, 2006; Khanal and Robinson, 2013). Information on the geometry of these subsurface structures has been used to construct kinematic models and structural cross-sections to calculate the amount of upper crustal shortening undergoing between the Sub-to-Higher Himalaya, and understand how convergence between the India and Eurasian plates is being accommodated. Most of these studies have been carried out in Uttarakhand and Nepal. A necessary feature found among most structural cross-sections is the accretion and piling up of Indian plate material against higher-grade rock (juxtaposed by the MCT), by sequence of southward propagating thrust ramps along the MHT. Over time, these ramps eventually become imbricate thrusts that give rise to crustal-scale duplexing occurring along the Himalayan arc (Lyon-Caen and

Molnar, 1983). This contrasts with simpler models that present the MHT as having a single major active ramp that connects the upper and lower planes of the MHT. As the duplex grows and evolves, it can be expressed at the surface as a hinterland dipping antiform unroofed by erosion that exposes the complex thrust sheets and folds within (Ahmad et al., 2000; Schelling and Arita, 1991). These surface observations have informed various balanced cross-sections, requiring a duplex structure of some expanse and configuration to be essential in accommodating north-south shortening in the Lesser Himalaya during the inter-seismic period of the MHT while it remains mostly locked.

Delineating the complex thrust geometries of duplexes at depth, as opposed to making (necessary) assumptions when drawing cross-sections based on surface observations, is more challenging. For one, a duplex will have to be well-developed and/or active enough for depth-probing geophysical methods to be able to image or map its architecture. Secondly, accuracy on the order of a few kilometers is required to distinguish the duplexes individual complex network of imbricate thrusts—which are comparatively much smaller than the surrounding crustal-scale thrusts like the MCT and MHT. For these reasons, structural geologists have often relied on earthquake locations and their focal mechanisms to help inform construction of balanced cross-sections. However, as mentioned earlier, few seismic networks have blanketed the Himalaya with adequate station coverage to capture enough well-constrained micro-seismicity capable of mapping duplexes in high resolution. Still, some seismological investigators have made substantial progress on this end in the recent decade. For example, Mahesh, S. Gupta, et al. (2015), Prasath, Paul, and S. Singh (2017), and Negi et al. (2017) used local and permanent stations in Uttarakhand to relo-

cate earthquakes and compute fault plane solutions, which predominantly indicate thrust type faulting dipping at angles significantly greater than the MHT below. By combining earthquake-based observations with geological interpretations, those studies infer the bulk of seismicity in the Lesser Himalaya to be associated with an MHT ramp, out-of-sequence thrust, a duplex structure, or some combination of each. In this study, although we use the same stations as those authors for the same time period, we are able to map a Lesser Himalayan duplex structure in high resolution. Important to note, though, is that we delineate a duplex only at this location in Uttarakhand and not elsewhere in the other examined cross-sections. This may be due to lateral structural variations of the duplex, or because it may not be sufficiently activated (e.g. by a large earthquake on the lower portion of the MHT) to produce enough seismicity throughout multiple thrusts.

From the duplex inferred beneath the Lesser Himalaya along profile C, we develop a refined 2-D geometry model of the MHT in Uttarakhand (Figure 3.4). To do this we consider other geophysical studies that have taken place in the immediate vicinity to constrain the down-dip and up-dip flat segments of the MHT—since seismicity is sparse in these areas of our earthquake catalog. Specifically, we turn to a study by Caldwell et al. (2013) who used the same network to em-ploy receiver functions techniques to image the subsurface down to 100 km depth. A direct com-parison with their results is possible because their experiment took place just 10-30 km away from our cross-section where the duplex is best observed, thus providing an excellent comparison for interpretations since the effects of along-strike structural variation is likely to be minimal. In the cross-section of Figure 3.4, we see a good fit between our interpreted duplex within the upper and lower planes

of Caldwell et al.'s MHT model. However, in this study we do not observe the same mid-crustal 16° dipping ramp interpreted by Caldwell et al. (2013). Instead, we infer at least two imbricate faults dipping at greater angles than a single major ramp, with the southernmost thrust possibly being the most current (active), more minor "ramp" in this area of the MHT. Combining multiple observations, we obtain a general 2-D model of the MHT that resembles a similar model of the MHT derived in central Nepal after the 2015 Gorkha earthquake aftershock sequence (M. Mendoza et al., 2019). A general description of this MHT model for Uttarakhand is as follows: at a depth of 10 km the upper flat of the MHT dips gently at 2°; transitions into a ∼10 km-wide and ∼40 km long Lesser Himalaya duplex architecture; then re-connects at 20 km depth to a 4° dipping lower flat plane MHT that extends northwards beneath the Higher Himalaya (Figure 3.4).

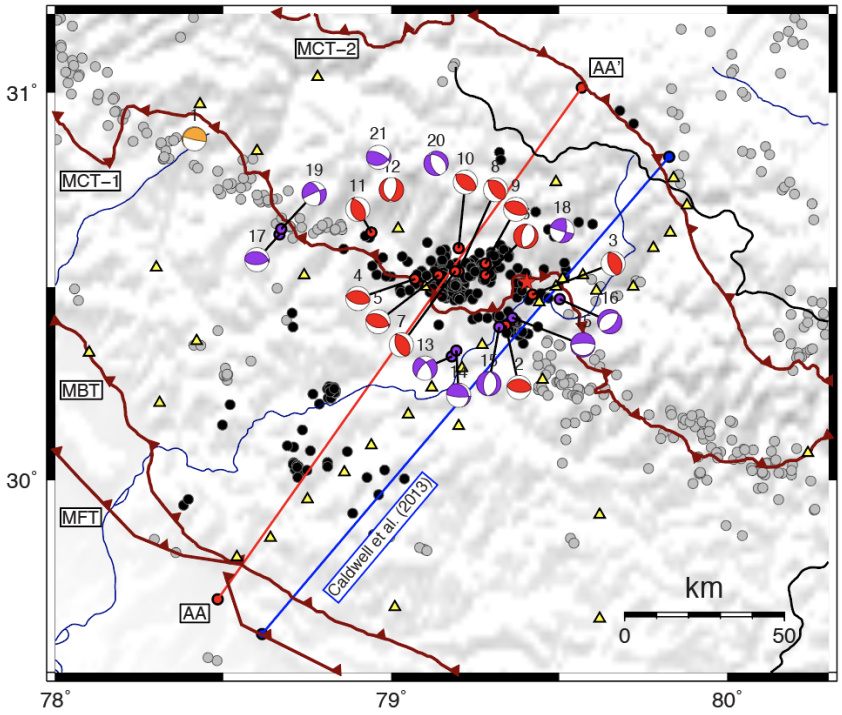
MCT–2
AA'
MCT–1
MBT
MFT
AA
Caldwell et al. (2013)
km
0
50
31°
30°
78°
79°
80°

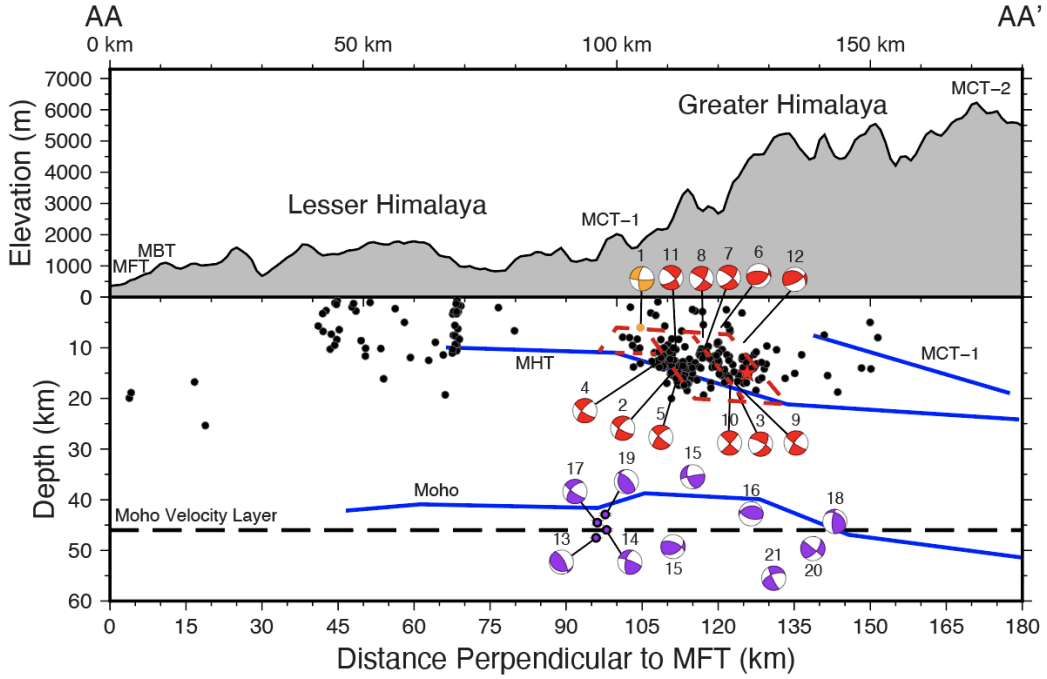
AA
AA'
0 km
50 km
100 km
150 km
Elevation (m)
Greater Himalaya
MCT–2
Lesser Himalaya
MCT–1
MBT
MFT
MHT
Moho
Moho Velocity Layer
Depth (km)
Distance Perpendicular to MFT (km)

Figure 3.4: (Top) Map view perspective showing earthquakes where we infer a duplex structure (Figure 2, profile C), plotted with focal mechanisms (red) obtained by Mahesh, S. Rai, et al. (2013) for events in the same area. The orange focal mechanism shown 90 km to the west was obtained by Negi et al. (2017), which he inferred to be associated with the Tons thrust sheet; i.e., the roof of a Lesser Himalaya duplex. Purple focal mechanisms represent the locations of the ten near-Moho earth-quakes scrutinized in this study. The blue profile line shows the location from which Caldwell et al. (2013) imaged crustal structures and the Moho using receiver function CCP stacking. All duplex-associated earthquakes, focal mechanisms, and inferred geometry profiles of the MFT, MCT, and Moho inferred by Caldwell et al. (2013) are projected onto profile line AA. (Bottom) Elevation profile showing major physiographic features of the Himalaya plotted above a cross-section containing the key points of this study. Above 25 km depth we provide a refined model of the MHT in Uttarakhand containing a duplex structure, corroborated by earthquake relocations and focal mechanisms At Moho depths, most focal mechanisms are of normal faulting type, which could be indicative of lower crust-upper mantle flexural bending; i.e., extension of the Indian plate as it underthrusts southern Tibet.

3.6 Lower crust and Upper Mantle Earthquakes in Western Himalaya

Seismicity recorded by the CSIR and WIHG joint network also reveal the existence of lower crust and potential upper mantle earthquakes in Uttarakhand. Previous studies using the same network have located sparse seismicity at these depths (Mahesh at al., 2013) and computed their fault plane solutions (Negi et al., 2017; Mahesh, S. Gupta, et al., 2015); however, here we compile more evidence of events occurring both above and below the Moho, to explore in greater detail the conditions that give rise to them.

Like the dense shallow band of seismicity discussed above, the near-moho earthquakes examined in this study are occurring beneath the physiographic transition from the Lesser to Higher Himalaya (Figure 3.4). It is around this area of the arc where it is inferred that the Indian lithosphere experiences flexural bending as it underthrusts the Himalayan mountains and Tibetan Plateau (Mahesh, S. Rai, et al., 2013; Gaspar Monsalve, McGovern, and A. Sheehan, 2009; De la Torre et al., 2007; Jordan and Watts, 2005). Studies that utilized the high-performance procedure of receiver function stacking in the Himalaya show a sub-horizontal Moho surface beneath the Sub to Higher Himalaya at a depth of ∼35 to 45 km (Schulte-Pelkum et al., 2005; Nábělek et al., 2009; Acton et al., 2011; Caldwell et al., 2013). As with our duplex model, to best guide interpretations of our focal mechanisms and the various faulting styles they represent, we adopt the Moho profile inferred by Caldwell et al. (2013) since it is: (1) imaged along a linear station transect less than 50 km east of profile line AA (Figure 3.4); and (2) because the Moho velocity layer used to determine hypocentral locations in our catalog is located at 46 km below sea level (Negi et al., 2017),

which is compatible with Caldwell et al.'s 45 km deep Moho and provides confidence on where our locations reside with respect to it.

In the following, we systematically interpret the faulting styles of ten small magnitude (0.97-3.34) earthquakes occurring at 30-60 km depth with respect to the Moho interpreted by Caldwell et al. (2013), to better understand the processes of brittle failure where it is thought to be rare or non-existent (Jackson, 2002). It is important to first note that we regard the Moho as a narrow zone of some laterally varying width, as shown by receiver function images (e.g., Caldwell et al., 2013; Nábělek et al., 2009; Schulte-Pelkum et al., 2005). This is kept in mind when interpret-ing focal mechanisms at their location with respect to the Moho, since different faulting styles (i.e. processes) could be expected for earthquakes occurring in the lower crust versus the lithospheric mantle. Our focal mechanisms indicate normal faulting to be the predominant style of deformation occurring beneath the Lesser Himalaya at near-Moho depths. Further, if we postulate that most fault planes at these depths are associated with N-S extension due to the Indian crust flexing con-cave down (Ni and Barazangi, 1984; Mahesh, S. Gupta, et al., 2015; Lyon-Caen and Molnar, 1983), the T-axis (extensional axis) of those normal faulting focal mechanisms appear to rotate from arc-perpendicular above the Moho to arc-parallel below it, possibly indicating a change in the orientation of principal stresses in the lithosphere with depth.

Beneath the Moho profile down to 55 km depths, three focal mechanisms indicate thrust-faulting with arc-perpendicular P-axes (compressional axes), where two of which have a small strike-slip component. Beneath the Ganga basin, the 1988 mb 6.5 Udaypur earthquake occurred approximately at the same depth (55 km) and exhibited the same

arc-perpendicular faulting (W.-P. Chen and Kao, 1996). Later observational (De la Torre et al., 2007) and modeling (Gaspar Monsalve, McGovern, and A. Sheehan, 2009) studies infer thrust faulting (N-S shortening) to be the predominant style of deformation near the Moho beneath the Ganga basin and Sub-Himalaya.

Adjacent to the Moho profile and separated about 45 km apart are two focal mechanisms exhibiting strike-slip faulting with roughly arc-perpendicular P-axes. This observation is consistent with earthquakes located beyond Moho depths beneath the Higher Himalaya and southern Tibet, but at 70 to 100 km depths (De la Torre et al., 2007; Monsalve et al., 2006; Zhu and Helmberger, 1996). Those focal mechanisms also exhibit strike-slip faulting with arc-perpendicular P-axis, suggesting that vertical plane shearing reflects the predominant orientation of strain at sub-Moho depths (De la Torre et al., 2007). Additionally, predicted principal stress orientations determined from flexural modeling of the Indian lithosphere (Gaspar Monsalve, McGovern, and A. Sheehan, 2009) closely match the focal mechanisms by De la Torre et al. (2007) at the same depths. This is of course in contrast to our observations beneath the Lesser Himalaya, specifically, where most focal mechanisms indicate normal faulting to be dominating.

The above focal mechanism analyses may suggest that at lower crust and upper mantle depths there is a transition in deformation styles where – by support of previous observations (Mahesh, S. Gupta, et al., 2015; De la Torre et al., 2007; Zhu and Helmberger, 1996) and models (Gaspar Monsalve, McGovern, and A. Sheehan, 2009)—there is: thrust-faulting (shortening) beneath the Ganga basin; normal faulting (extension) beneath the Sub- and Lesser Himalaya due to flexural bending; followed by strike-slip faulting beneath the

Higher Himalaya and Tibet. The assortment of focal mechanisms we obtain may be reflective of the complex and indiscrete transition of deformation styles along arc-perpendicular distances near the Moho. However, given that most of our focal mechanisms beneath the Lesser Himalaya are of normal faulting type, this could be an indicator of where flexural bend-ing is starting to take place. Other factors contributing to the apparent "mixed-bag" of faulting styles exhibited by our focal mechanisms could be owed to local homogeneities and lateral varia-tions in elastic properties at scales akin to those small magnitude earthquakes, or by pockets of fluids being generated in the upper mantle through metamorphic reactions and underplating (Gaspar Monsalve, McGovern, and A. Sheehan, 2009; Nábělek et al., 2009; Jackson et al., 2004). To this end, the observations interpreted here and in previous works seem to contradict the notion made by Jackson (2002) and others that all earthquakes are confined to the crust, above the Moho.

3.7 Conclusions

Observations of small-to-moderate sized earthquakes indicate dynamic processes taking place throughout the Indian lithosphere beneath the Lesser Himalaya. In Uttarakhand we develop a robust earthquake catalog and compare it with other geophysical observations to help reconcile long-debated topics surrounding Himalayan tectonics. In the upper crust, we show evidence that the MHT has a duplex-style architecture, as first introduced by some of the earliest geological cross-sections constructed from surficial observations in different parts of the Himalayas. Seismological confirmation of a Lesser Himalayan duplex documented in high-resolution in central Nepal (M. Mendoza et al., 2019), and in this study,

promotes the idea that such a prominent structural feature might be prevalent across the length of the Himalayas. If so, this offers important insight into how the Lesser Himalaya is accommodating plate convergence via active shortening during the inter-seismic period, and controlling the nucleation and rupture process of large earthquakes. Beneath the MHT, we infer the existence of brittle failure taking place down to the lithospheric mantle, a phenomenon in this tectonic setting that had only been properly documented in eastern Nepal until now. Focal mechanisms suggest extension may be the predominant style of deformation occurring at 30-60 km depth beneath the Lesser Himalaya due to flexural bending of the Indian plate. If so, this could help to inform Himalayan kinematic and deformation models, and improve our under-standing of large-scale orogenic processes in general.

Bibliography

Acton, CE et al. (2011). "Crustal structure of the Darjeeling—Sikkim Himalaya and southern Tibet". In: *Geophysical Journal International* 184.2, pp. 829–852.

Ader, Thomas et al. (2012). "Convergence rate across the Nepal Himalaya and interseismic coupling on the Main Himalayan Thrust: Implications for seismic hazard". In: *Journal of Geophysical Research: Solid Earth* 117.B4.

Adhikari, Lok Bijaya et al. (2021). "Orogenic collapse and stress adjustments revealed by an intense seismic swarm following the 2015 Gorkha earthquake in Nepal". In: *Frontiers in Earth Science*, p. 524.

Ahmad, Talat et al. (2000). "Isotopic constraints on the structural relationships between the lesser Himalayan series and the high Himalayan crystalline series, Garhwal Himalaya". In: *Geological Society of America Bulletin* 112.3, pp. 467–477.

Arora, Baldev Raj et al. (2007). "A peep into the himalayan seismicity". In: Indian Geological Congress.

Bai, Ling et al. (2019). "Lateral variation of the Main Himalayan Thrust controls the rupture length of the 2015 Gorkha earthquake in Nepal". In: *Science advances* 5.6, eaav0723.

Baillard, Christian et al. (2017). "Automatic analysis of the Gorkha earthquake aftershock sequence: Evidences of structurally segmented seismicity". In: *Geophysical Journal International* 209.2, pp. 1111–1125.

Bilham, Roger (2019). "Himalayan earthquakes: a review of historical seismicity and early 21st century slip potential". In: *Geological Society, London, Special Publications* 483.1, pp. 423–482.

Bollinger, Laurent et al. (2014). "Estimating the return times of great Himalayan earthquakes in eastern Nepal: Evidence from the Patu and Bardibas strands of the Main Frontal Thrust". In: *Journal of Geophysical Research: Solid Earth* 119.9, pp. 7123–7163.

Caldwell, Warren B et al. (2013). "Characterizing the Main Himalayan Thrust in the Garhwal Himalaya, India with receiver function CCP stacking". In: *Earth and Planetary Science Letters* 367, pp. 15–27.

Chen, W-P and H Kao (1996). "Seismotectonics of Asia: Some recent progress". In: *WORLD AND REGIONAL GEOLOGY* 1.8, pp. 37–62.

Dal Zilio, Luca et al. (2019). "Bimodal seismicity in the Himalaya controlled by fault friction and geometry". In: *Nature communications* 10.1, pp. 1–11.

De la Torre, TL et al. (2007). "Earthquake processes of the Himalayan collision zone in eastern Nepal and the southern Tibetan Plateau". In: *Geophysical Journal International* 171.2, pp. 718–738.

DeCelles, PG et al. (1998). "Neogene foreland basin deposits, erosional unroofing, and the kinematic history of the Himalayan fold-thrust belt, western Nepal". In: *Geological Society of America Bulletin* 110.1, pp. 2–21.

Elliott, JR et al. (2016). "Himalayan megathrust geometry and relation to topography revealed by the Gorkha earthquake". In: *Nature Geoscience* 9.2, pp. 174–180.

Fukuyama, Eiichi et al. (2003). "Detailed fault structure of the 2000 western Tottori, Japan, earthquake sequence". In: *Bulletin of the Seismological Society of America* 93.4, pp. 1468–1478.

Gualandi, Adriano et al. (2017). "Pre-and post-seismic deformation related to the 2015, Mw7. 8 Gorkha earthquake, Nepal". In: *Tectonophysics* 714, pp. 90–106.

Hardebeck, Jeanne L and Peter M Shearer (2008). *HASH: A FORTRAN Program for Computing Earthquake First-Motion Focal Mechanisms–v1. 2–January 31, 2008.*

Jackson, JA (2002). "Strength of the continental lithosphere: time to abandon the jelly sandwich?" In: *GSA today* 12, pp. 4–10.

Jackson, JA et al. (2004). "Metastability, mechanical strength, and the support of mountain belts". In: *Geology* 32.7, pp. 625–628.

Jordan, TA and AB Watts (2005). "Gravity anomalies, flexure and the elastic thickness structure of the India–Eurasia collisional system". In: *Earth and Planetary Science Letters* 236.3-4, pp. 732–750.

Karplus, Marianne S et al. (2020). "A rapid response network to record aftershocks of the 2015 M 7.8 Gorkha earthquake in Nepal". In: *Seismological Research Letters* 91.4, pp. 2399–2408.

Kayal, JR et al. (2003). "Aftershocks of the March 1999 Chamoli earthquake and seismotectonic structure of the Garhwal Himalaya". In: *Bulletin of the Seismological Society of America* 93.1, pp. 109–117.

Khanal, Subodha and Delores M Robinson (2013). "Upper crustal shortening and forward modeling of the Himalayan thrust belt along the Budhi-Gandaki River, central Nepal". In: *International Journal of Earth Sciences* 102.7, pp. 1871–1891.

Kumar, Naresh, Ajay Paul, et al. (2012). "The Mw 5.0 Kharsali, Garhwal Himalayan earthquake of 23 July 2007: source characterization and tectonic implications". In: *Curr Sci* 102.12, pp. 1674–1682.

Kumar, Naresh, Jyoti Sharma, et al. (2009). "Seismotectonic model of the Kangra–Chamba sector of northwest Himalaya: Constraints from joint hypocenter determination and focal mechanism". In: *Bulletin of the Seismological Society of America* 99.1, pp. 95–109.

Kumar, Senthil et al. (2001). "Earthquake recurrence and rupture dynamics of Himalayan Frontal Thrust, India". In: *Science* 294.5550, pp. 2328–2331.

Lyon-Caen, Hélène and Peter Molnar (1983). "Constraints on the structure of the Himalaya from an analysis of gravity anomalies and a flexural model of the lithosphere". In: *Journal of Geophysical Research: Solid Earth* 88.B10, pp. 8171–8191.

Macfarlane, AM, KV Hodges, and D Lux (1992). "A structural analysis of the Main Central thrust zone, Langtang National Park, central Nepal Himalaya". In: *Geological Society of America Bulletin* 104.11, pp. 1389–1402.

Mahesh, P, Sandeep Gupta, et al. (2015). "Seismotectonics and crustal stress field in the Kumaon–Garhwal Himalaya". In: *Tectonophysics* 655, pp. 124–138.

Mahesh, P, SS Rai, et al. (2013). "One-dimensional reference velocity model and precise locations of earthquake hypocenters in the Kumaon–Garhwal himalaya". In: *Bulletin of the Seismological Society of America* 103.1, pp. 328–339.

Mendoza, MM et al. (2019). "Duplex in the Main Himalayan Thrust illuminated by aftershocks of the 2015 M w 7.8 Gorkha earthquake". In: *Nature Geoscience* 12.12, pp. 1018–1022.

Monsalve, G et al. (2006). "Seismicity and one-dimensional velocity structure of the Himalayan collision zone: Earthquakes in the crust and upper mantle". In: *Journal of Geophysical Research: Solid Earth* 111.B10.

Monsalve, Gaspar, Patrick McGovern, and Anne Sheehan (2009). "Mantle fault zones beneath the Himalayan collision: Flexure of the continental lithosphere". In: *Tectonophysics* 477.1-2, pp. 66–76.

Mousavi, S Mostafa et al. (2020). "Earthquake transformer—an attentive deep-learning model for simultaneous earthquake detection and phase picking". In: *Nature communications* 11.1, pp. 1–12.

Mugnier, J-L et al. (2013). "Structural interpretation of the great earthquakes of the last millennium in the central Himalaya". In: *Earth-Science Reviews* 127, pp. 30–47.

Nábělek, John et al. (2009). "Underplating in the Himalaya-Tibet collision zone revealed by the Hi-CLIMB experiment". In: *Science* 325.5946, pp. 1371–1374.

Negi, Sanjay S et al. (2017). "Crustal velocity structure and earthquake processes of Garhwal-Kumaun Himalaya: Constraints from regional waveform inversion and array beam modeling". In: *Tectonophysics* 712, pp. 45–63.

Ni, James and Muawia Barazangi (1984). "Seismotectonics of the Himalayan collision zone: Geometry of the underthrusting Indian plate beneath the Himalaya". In: *Journal of Geophysical Research: Solid Earth* 89.B2, pp. 1147–1163.

Paige, Christopher C and Michael A Saunders (1982). "LSQR: An algorithm for sparse linear equations and sparse least squares". In: *ACM Transactions on Mathematical Software (TOMS)* 8.1, pp. 43–71.

Pavlis, Gary L et al. (2004). "The generalized earthquake-location (GENLOC) package: An earthquake-location library". In: *Computers & Geosciences* 30.9-10, pp. 1079–1091.

Prasath, R Arun, Ajay Paul, and Sandeep Singh (2017). "Upper crustal stress and seismotectonics of the Garhwal Himalaya using small-to-moderate earthquakes: implications to the local structures and free fluids". In: *Journal of Asian Earth Sciences* 135, pp. 198–211.

Prasath, R Arun, Ajay Paul, and Sandeep Singh (2019). "Earthquakes in the Garhwal Himalaya of the Central seismic gap: A study of historical and present seismicity and their implications to the seismotectonics". In: *Pure and Applied Geophysics* 176.11, pp. 4661–4685.

Rajendran, CP and Kusala Rajendran (2005). "The status of central seismic gap: a perspective based on the spatial and temporal aspects of the large Himalayan earthquakes". In: *Tectonophysics* 395.1-2, pp. 19–39.

Rajendran, Kusala, Revathy M Parameswaran, and CP Rajendran (2018). "Revisiting the 1991 Uttarkashi and the 1999 Chamoli, India, earthquakes: Implications of rupture mechanisms in the central Himalaya". In: *Journal of Asian Earth Sciences* 162, pp. 107–120.

Robinson, Delores M, Peter G DeCelles, and Peter Copeland (2006). "Tectonic evolution of the Himalayan thrust belt in western Nepal: Implications for channel flow models". In: *Geological Society of America Bulletin* 118.7-8, pp. 865–885.

Saklani, PS, DC Nainwal, and VK Singh (1991). "Geometry of the composite Main Central Thrust (MCT) in the Yamuna Valley, Garhwal Himalaya, India". In: *N. Jb. Geol. Palaont. Mh* 1991, pp. 364–380.

Satyabala, SP and Roger Bilham (2006). "Surface deformation and subsurface slip of the 28 March 1999 Mw= 6.4 west Himalayan Chamoli earthquake from InSAR analysis". In: *Geophysical Research Letters* 33.23.

Schelling, Daniel and Kazunori Arita (1991). "Thrust tectonics, crustal shortening, and the structure of the far-eastern Nepal Himalaya". In: *Tectonics* 10.5, pp. 851–862.

Schulte-Pelkum, Vera et al. (2005). "Imaging the Indian subcontinent beneath the Himalaya". In: *Nature* 435.7046, pp. 1222–1225.

Seeber, L and JG Armbruster (1984). "Some elements of continental subduction along the Himalayan front". In: *Tectonophysics* 105.1-4, pp. 263–278.

Sheehan, Anne F et al. (2008). "Earthquakes and crustal structure of Himalaya from Himalayan Nepal-Tibet seismic experiment (HIMNT)". In: *Journal of Nepal Geological Society* 38, pp. 1–8.

Srivastava, HN et al. (2015). "Discriminatory characteristics of seismic gaps in Himalaya". In: *Geomatics, Natural Hazards and Risk* 6.3, pp. 224–242.

Srivastava, Praveen and Gautam Mitra (1994). "Thrust geometries and deep structure of the outer and lesser Himalaya, Kumaon and Garhwal (India): Implications for evolution of the Himalayan fold-and-thrust belt". In: *Tectonics* 13.1, pp. 89–109.

Stevens, VL and J-P Avouac (2016). "Millenary Mw¿ 9.0 earthquakes required by geodetic strain in the Himalaya". In: *Geophysical Research Letters* 43.3, pp. 1118–1123.

Vorobieva, Inessa, Prantik Mandal, and Alexander Gorshkov (2017). "Block-and-fault dynamics modelling of the Himalayan frontal arc: Implications for seismic cycle, slip deficit, and great earthquakes". In: *Journal of Asian Earth Sciences* 148, pp. 131–141.

Waldhauser, Felix and William L Ellsworth (2000). "A double-difference earthquake location algorithm: Method and application to the northern Hayward fault, California". In: *Bulletin of the Seismological Society of America* 90.6, pp. 1353–1368.

Xu, Wenbin, Roland Bürgmann, and Zhiwei Li (2016). "An improved geodetic source model for the 1999 M W 6.3 Chamoli earthquake, India". In: *Geophysical Supplements to the Monthly Notices of the Royal Astronomical Society* 205.1, pp. 236–242.

Zhu, Lupei and Donald V Helmberger (1996). “Intermediate depth earthquakes beneath the India-Tibet collision zone”. In: *Geophysical Research Letters* 23.5, pp. 435–438.

Chapter 4

Dynamic Triggering of Small Local Earthquakes in the Central Himalaya

4.1 Abstract

We present the first observation of remote dynamic triggering of local microearthquakes in the central Himalaya caused by the teleseismic waves from the 2007 M_w 8.5 Sumatra earthquake that occurred ∼4500 km away. We find small local earthquakes in the Kumaon-Garhwal Himalaya triggered by teleseismic long-period surface waves. Interestingly, an elevated level of seismicity persists for a week or so after the arrival of the teleseismic waves. The teleseismic waves impart ∼9 kPa of peak dynamic stresses, suggesting that the Himalayan faults in this area are sensitive to small stress changes. This heightened

and protracted seismicity indicates that the transient dynamic stresses may have triggered secondary processes, such as slow slip, that may be responsible for the persistence of this earthquake sequence. The region is thought to be close to a large damaging earthquake in the near future. This study provides improved constraints on the factors controlling the earthquake cycle.

4.2 Introduction

The boundary between the India and Eurasia plates has a history of major and great earthquakes. The most recent earthquake in this region is the 2015 M_w 7.8 Gorkha earthquake, which killed over 8700 people from a combination of infrastructure failure and triggered landslides (Bilham, 2015). Prior to the event, this segment of Himalaya was inferred to have a slip deficit of 4 m (Bilham, Gaur, and Molnar, 2001). Just a couple hundred kilometers away to the northwest, Kumaon-Garhwal Himalaya is inferred to have the same 4 m slip deficit, and capable of producing a M_w 8.0 or greater earthquake (C. Rajendran and K. Rajendran, 2005). It is in dangerous proximity to incredibly densely populated areas including the second most populated city in the world, New Delhi, home to approximately 16 million people. Because of the devastating impact of the Gorkha event in Nepal, it is more crucial than ever to investigate the state of stress in this 500–800 km long unruptured segment of the Himalayan arc that is referred to as the Kumaon-Garhwal "central seismic gap" (C. Rajendran and K. Rajendran, 2005). The most recent major earthquake in this area is a M_w 7.7 event, which occurred in 1803 and was not a plate-boundary-type event (C. Rajendran and K. Rajendran, 2005). Therefore, it is believed

that the region is currently in a quiescence, where a great (>M 8) earthquake has not occurred here in over 1000 years (C. Rajendran and K. Rajendran, 2005).

Due to thinly dispersed seismic networks and lack of broadband stations in the past, knowledge of the fault properties, geometry, and spatiotemporal distribution of earthquakes in this part of the Himalayas is insufficient for a comprehensive understanding of the fault system. However, relatively recent data from a high-resolution broadband seismic network operating between 2005 and 2012 in Kumaon-Garhwal, India, provides an excellent opportunity to study this region in detail. Here we present the first evidence of protracted local microearthquake activity in this area, dynamically triggered by the 2007 M_w 8.5 Sumatra earthquake, an event located ~4500 km away (Figure 4.1). Observations of dynamically triggered small local earthquake are well documented in many places (e.g., S. Prejean et al., 2004; Stephanie G Prejean, Hill, and Myers, 2010). For example, the M_w 7.9 Denali Fault earthquake clearly shows the rapid onset of dynamically triggered microseismicity up to 3660 km away. Considering how static stresses diminish more rapidly than dynamic stresses with increasing distance, previous observations and laboratory experiments attribute earthquake triggering to be dependent on load amplitude, rate, and duration of transient long-period surface wave perturbations, that can overcome the frictional strength and normal clamping of a near-failure fault (Van Der Elst and Savage, 2015; Gomberg, Beeler, et al., 1998). On the other hand, Hill (2008) found that fault geometry and incidence angle of seismic waves play a major role in governing remote triggering. Additionally, his study suggests that thrust faults, which essentially define the Himalayas, must be more susceptible to dynamic triggering by Rayleigh waves than normal faults in

the shallower portion of the crust. There is still no fully satisfactory answer that explains the rapid onset of remote triggering, let alone secondary processes that may explain delayed triggering after the passage of teleseismic surface waves. Understanding the state of stress and mechanisms that control the earthquake cycles in a given region is crucial.

Studying dynamic triggering in this continental-continental thrust regime can give new insights into physical processes responsible for earthquake generation such as: fluid pressure, stress heterogeneities, fault geometries, stress transfer, and fault frictional properties, to name a few. In this study, we analyze dynamic stresses from the passage of large teleseismic waves and characterize the resulting seismic activity in space and time to better constrain stress sensitivity of the faults and mechanisms governing remote triggering in the Kumaon-Garhwal seismogenic zone.

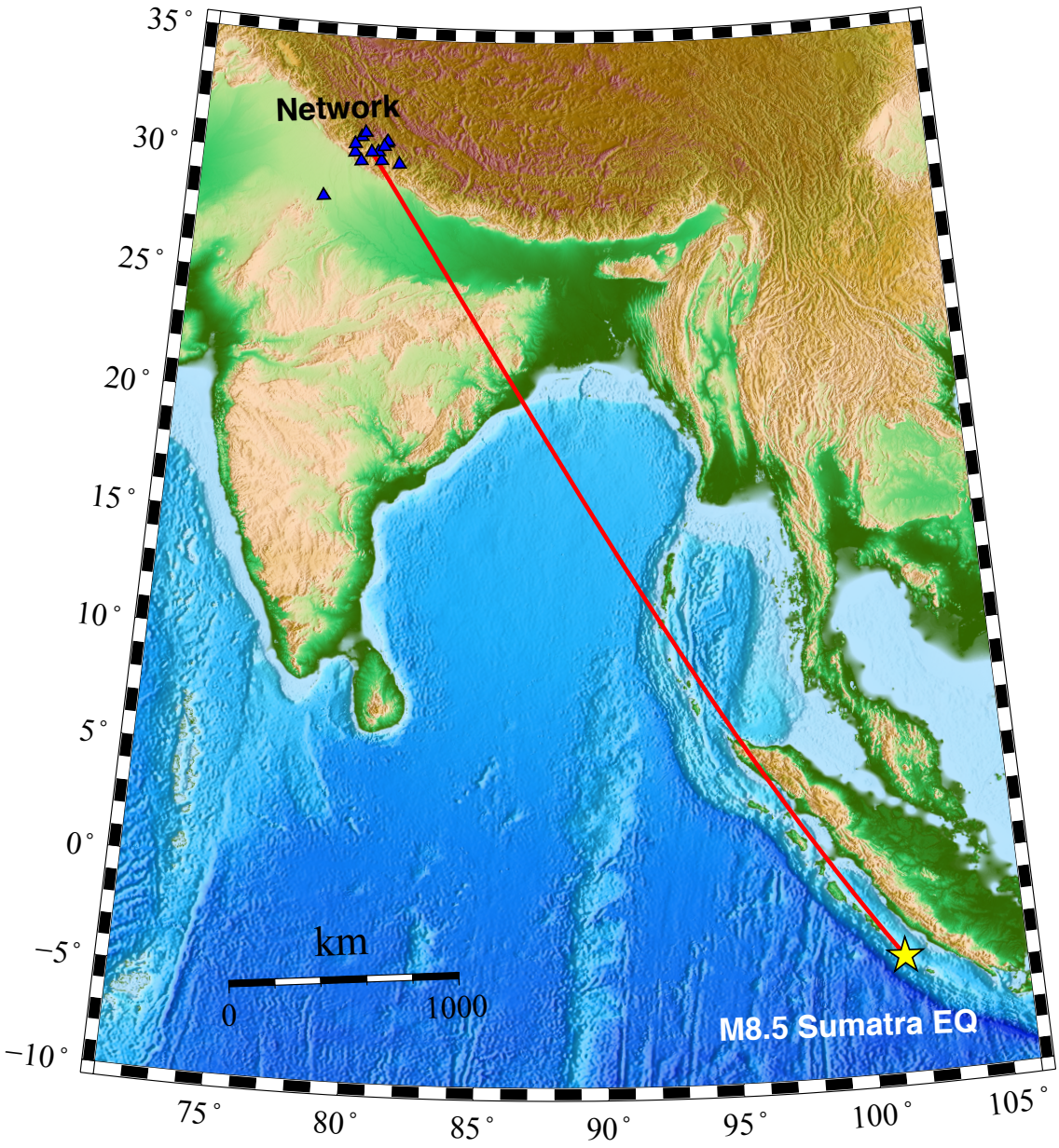

Figure 4.1: Map showing the location of the 2007 M_w 8.5 Sumatra earthquake and the seismic network in Kumaon-Garhwal, India, separated by a distance of 4500 km.

4.3 Methods

Continuous seismic waveform data used in this investigation come from a broad-band network consisting of 50 seismometers that were deployed for 6 years between 2005–2008 and 2011–2012 mainly north of the Main Frontal Thrust in the Kumaon-Garhwal region, India. The stations are distributed with 10–50 km spacing in a 60,000 km^2 area, extending 200 km in north-south and 300 km in east-west. There is one relatively isolated station 250 km south of the main network. Thirteen stations are operational during the time period investigated in this study. Mahesh et al. (2013) describes the details of the network. We visually inspect the continuous waveform data from the Kumaon-Garhwal network around the time of the Sumatra event to look for triggered local seismicity then carefully compare local seismic activity 15 days before and after the teleseismic event. The seismograms are analyzed at bandpass 1–5 Hz and 5–15 Hz, for any local seismicity within ∼120 km (S minus P time of ∼15 s) of the centermost station (GTH) in the network. Local events are placed into a "detection" catalog, whereas regional and teleseismic events are rejected. All detected events are checked in both horizontal and vertical components and at other frequencies to rule out distant events and noise. After scanning 30 days of continuous waveforms surrounding the Sumatra event, P and S phases are manually picked and used to locate events in Hypoinverse (Klein, 2002). Initial locations are then relocated using the HypoDD (Waldhauser and Ellsworth, 2000) algorithm. Both location programs use a local 1-D velocity model obtained by Mahesh et al. (2013). Events that are relocated using both P and S phases and recorded by at least three stations are then saved in a "location" catalog for further analyses.

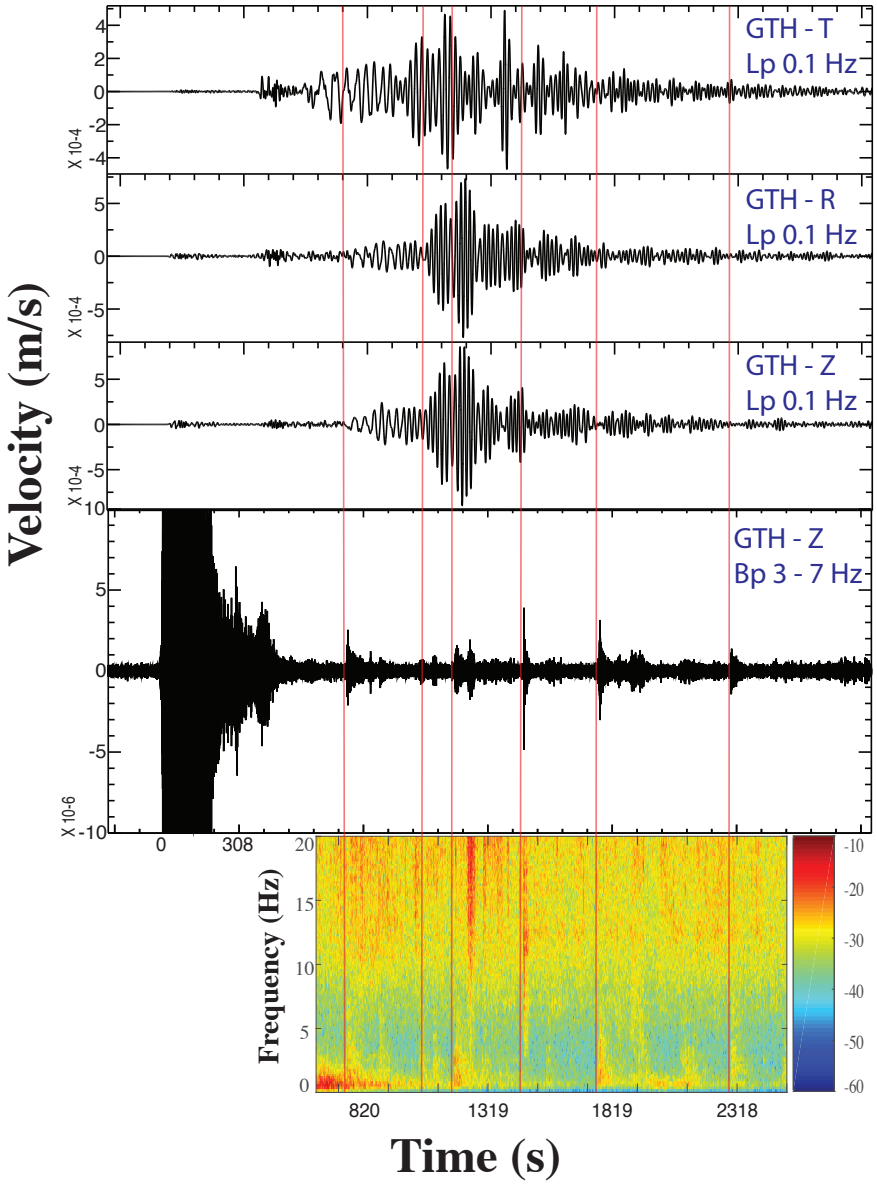

Figure 4.2: The 47 min time window showing dynamic triggering band-passed at 3–7 Hz and the surface wave train of the Sumatra event low-passed at 0.1 Hz in all channels. A spectrogram (bottom) also shows six local earthquakes that are observed to be dynamically triggered by both the Love and Rayleigh surface waves. Warm colors represent strong signal amplitude, whereas cooler colors represent weaker signal amplitude.

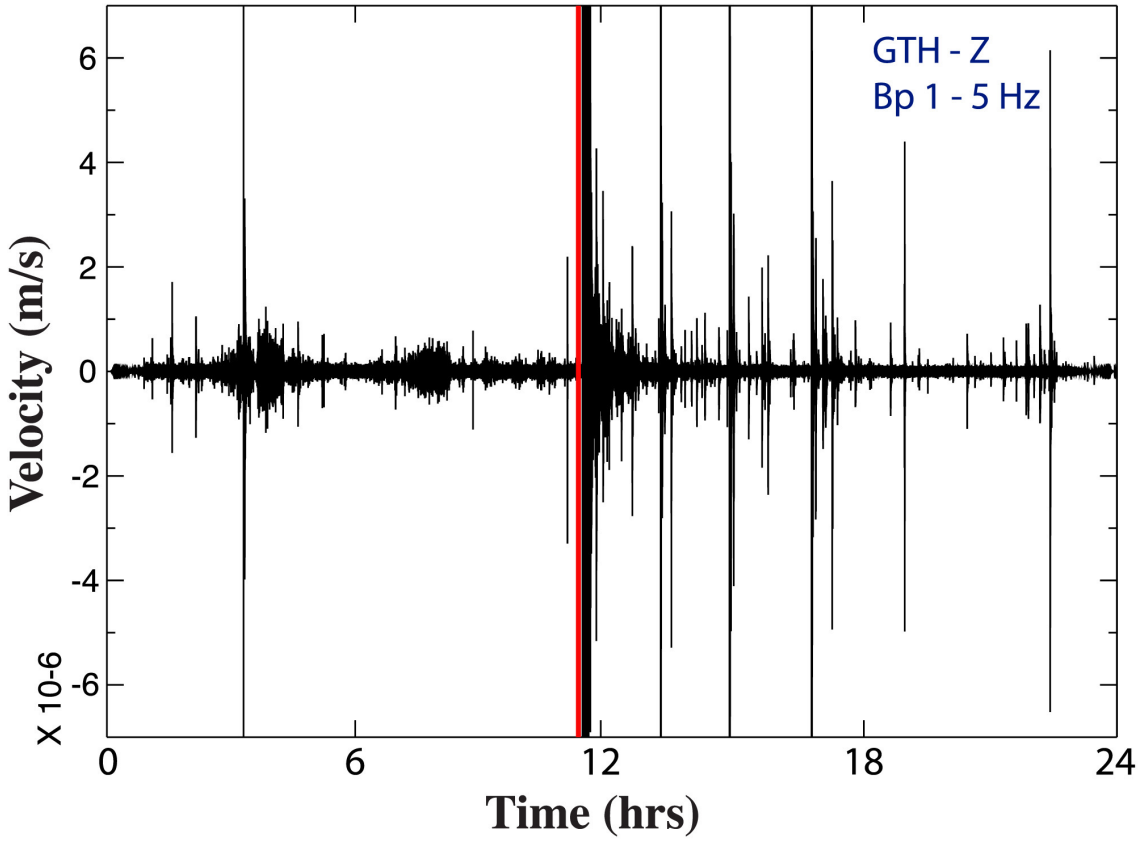

Figure 4.3: The 12 h before-and-after time window surrounding the 2007 Sumatra event (red), showing a dramatic increase in seismicity with amplitude versus time. The first large amplitude spike is the teleseismic P wave, which is rich in high frequencies and arrives at the station at a time of 11:18 h.

4.4 Results

Dynamically triggered local earthquakes in Kumaon-Garhwal by the teleseismic event are shown in the seismogram (Figure 4.2) recorded by the centermost station, GTH. The waves from the teleseismic event are shown at low-pass 0.1 Hz, whereas the higher frequency-rich local events are best observed between 1 and 5 Hz. During a half-an-hour time window of surface waves, six local events are dynamically triggered. A 1 day long seismogram (Figure 4.3) for station GTH, band passed at 1–5 Hz, shows a dramatic increase

in local seismicity starting immediately after the arrival of teleseismic waves. In fact, there is a six-fold increase in the number of earthquakes within 12 h starting immediately following the arrival of teleseismic waves, compared to the 12 h immediately before it. We detect 40 local events within 12 h after the arrival of waves from the teleseismic event, as opposed to six local events that occur 12 h prior. In addition, an elevated rate of seismic activity persists days after the passage of the teleseismic waves from the Sumatra event (Figure 4.4). Preceding the arrival of the teleseismic waves, there was an average of three local earthquakes per day, whereas an average of eight earthquakes that occur per day after, based on our detection catalog for 30 days around the teleseismic event. After the initial surge, seismicity gradually returns to the background level over the course of the next 7 days or so. Earthquakes 10 days before and after the arrival of the teleseismic event are shown in both map and cross-section view (Figure 4.5). In conjunction with the increased seismicity, we observe two distinct earthquake clusters in the central and southeastern part of the network.

In order to further investigate the triggering phenomenon, we calculate the dynamic stress imparted by the teleseismic waves in this area using the peak dynamic strain equation (Van Der Elst and Brodsky, 2010; Love, 2013) $\epsilon \approx \mathrm{V}/\mathrm{C}_s$, where ϵ is strain, V is the peak particle velocity from a seismogram, and C_s is surface wave velocity, a 3.2 km/s Rayleigh wave in this case. Love and Rayleigh waves can both trigger earthquakes (Hill, 2008), as observed in this study, but here we use a typical Rayleigh wave velocity since it shows the largest peak ground velocity of 0.001 m/s on the networks centermost station. The calculated dynamic stress is then obtained from multiplying the dynamic strain by a

commonly used shear modulus value of 30 GPa. For those earthquakes that are inferred to be dynamically triggered, we calculate dynamic stress imparted by the peak ground motion of Rayleigh waves to be ∼9 kPa.

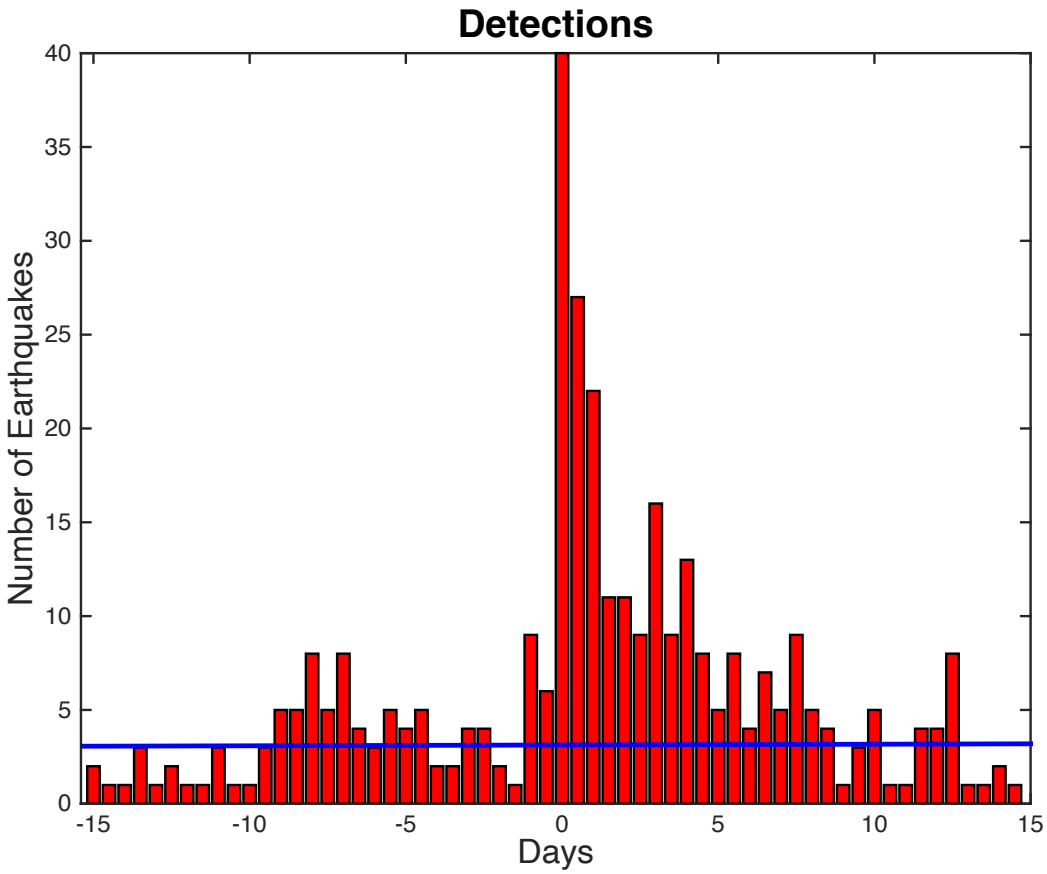

Figure 4.4: Histogram with 12 h bins of detected local earthquakes 15 days before and after the arrival of the 2007 Sumatra event. The blue line represents the average background seismicity before the teleseismic event. Locally triggered earthquakes begin ∼13 min after the arrival of the teleseismic P wave.

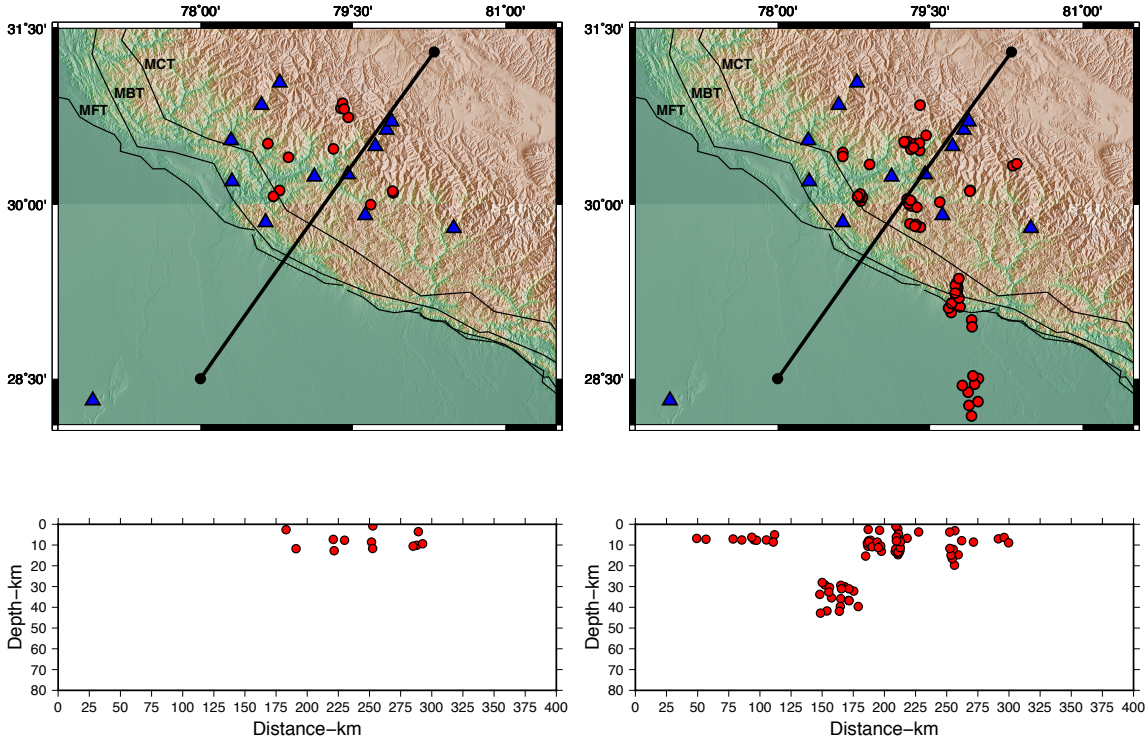

Figure 4.5: Map of stations (triangle) and relocated events (circle) in Kumaon-Garhwal, India. Seismicity is shown 10 days before (left), and 10 days after (right) the passage of the 2007 Sumatra event. It is important to note that clustering is more apparent after the event in comparison to before it.

4.5 Discussion

The extent to which dynamic stresses control the earthquake cycle on a fault, or population of faults, is still not well understood. Some, but not all, contributing physical processes to consider are as follows: pore fluid pressure, stress heterogeneities, fault geometry, frictional properties of the fault, and directivity effects (Brodsky and Van Der Elst, 2014; Gomberg, Reasenberg, et al., 2001; Hill, 2008). In the scope of this article, we do not investigate all of these possibilities. Based on the observations in this study, we argue that those dynamically triggered earthquakes occurred because the teleseismic waves had a

significant effect on the local coulomb stress field to allow the faults to be brought closer to failure. With a source-to-site distance of about 4500 km, our estimated dynamic stress of 0.009 MPa is consistent with previously observed dynamic stresses associated with remote triggering, ranging between ∼0.01 and <1 MPa (S. Prejean et al., 2004). Although stress imparted by seismic waves is small compared to tectonic stress, the most straightforward interpretation for the occurrence of dynamic triggering in this region is due to the combination of both dynamic and ambient stresses pushing faults over the Coulomb failure criteria, especially if those faults are optimally orientated with the stress oscillations of the transient waves. One such experimentally developed model that helps support this onset of dynamic triggering is clock advancement (Gomberg, Beeler, et al., 1998). Heuristic spring-slider analytical models explain how faults already subjected to continuous loading of the background static stresses are advanced in time to fail by the additional loading of dynamic stresses. For instance, when a population of faults at varying times within their earthquake cycles is subjected to dynamic loading, faults that are older in their cycle will experience more clock advancement to failure than those earlier in their cycle. The experiments concluded that the increase in seismicity due to clock advance only occurs during the period of transient disturbance, i.e., the passage of teleseismic waves. After this period of triggered events during the passage of teleseismic waves, a quiescence should follow until the background rate of seismicity is returned.

Although our results show an increase in local seismicity during the transient period, suggesting the clock advancement of the most critically stressed faults, this model does not explain the protracted elevated level of seismicity that lasts for at least a week. For this

reason, we consider local processes initiated by dynamic stresses that might have regulated the protracted level of heightened seismicity in central Himalaya. A possible scenario is that the dynamic stresses, induced by the propagating teleseismic waves, triggered local creep or slow slip along the faults in the area, a process that lasted for several days. Slow slip events (SSEs) have been found in a variety of tectonic environments to redistribute the stress locally and trigger small regular earthquakes, lasting from several hours to a week, as the SSE evolves in space and time (Delahaye et al., 2009; Peng and Joan Gomberg, 2010; Vidale et al., 2011). Slow slip is often associated with characteristic seismic signals, most commonly tectonic tremor (Ghosh et al., 2015; Peng and Joan Gomberg, 2010; Zhang et al., 2011). We, however, find no evidence of tremor activity produced during the time period of this study, through visual analyses of seismograms at multiple band passes. Nonetheless, SSEs have been observed without detectable tremor (Delahaye et al., 2009) and remain geodetically undetected unless they are sufficiently large and shallow (Smith and Joan Gomberg, 2009). Given that slow slip responds to extremely tiny stresses (Thomas et al., 2013), we infer that slow slip may be responsible for the protracted nature of elevated seismicity.

There are other physical processes that may be operating in this area and may explain the observations presented here. A cascade model may be particularly appealing in this regard. Once an earthquake is dynamically triggered, it can initiate a secondary process by loading surrounding faults with their own local static and dynamic stresses, setting off a cascade of earthquake sequences, or swarm, where no main shock is apparent (Brodsky and Van Der Elst, 2014). If a locally triggered event triggers additional events, this implies that some form of stress transfer is taking place along faults, or between them. Therefore,

areas of relieved and accumulated stress can in part be illustrated from the spatiotemporal distribution of earthquake locations after the passage of the transient waves (Figure 4.5). Coulomb failure stress and cascade models share a common ground in explaining the underlying mechanisms for the generation of triggered earthquakes and protracted elevated level of seismic activity even after the dynamic stresses diminish. Interestingly, the observations presented here are reminiscent of typical aftershock behavior at great distances where dynamic stresses from surface waves are dominant. This was observed when the M_w 7.9 Denali Fault earthquake remotely triggered small earthquakes and elevated levels of seismicity as far as 3660 km for up to 3 weeks (Pankow et al., 2004). In Baja California, the 2011 Tohoku event triggered seismic swarms, or a cascading sequence, for a couple of days that included two M>5 events (Gonzalez-Huizar et al., 2012).

Although we invoke clock advance, slow slip, and the cascade model that can possibly explain our observations, in reality it is possible that multiple processes are operating simultaneously and responsible for the dynamically triggered and protracted earthquake sequence reported here.

4.6 Conclusion

This study presents the first evidence of remotely triggered local microearthquakes in the Kumaon-Garhwal Himalaya, a segment of the Himalayan fault system also known as the "central seismic gap." During the passage of the teleseismic waves from the 2007 M_w 8.5 Sumatra earthquake, we show that peak transient dynamic shear stresses of $\sim$9 kPa are capable of dynamically triggering small local earthquakes in this region. There is

a six-fold increase in local seismicity in the first 12 h immediately following the arrival of teleseismic waves. In addition, the elevated level of seismicity is sustained for a week or so before it gradually decays back down to the background rate. We argue that secondary mechanisms are driving the near 10 day long increased level of local seismic activity in the central Himalaya. This investigation contributes to our understanding of the underlying physical processes that are likely influencing the state of stress and earthquake cycle in the Himalayas, and is critical in identifying conditions necessary for triggering earthquakes in a variety of tectonic environments.

Bibliography

Bilham, Roger (2015). "Raising Kathmandu". In: *Nature Geoscience* 8.8, pp. 582–584.

Bilham, Roger, Vinod K Gaur, and Peter Molnar (2001). "Himalayan seismic hazard". In: *Science* 293.5534, pp. 1442–1444.

Brodsky, Emily E and Nicholas J Van Der Elst (2014). "The uses of dynamic earthquake triggering". In: *Annual Review of Earth and Planetary Sciences* 42, pp. 317–339.

Delahaye, EJ et al. (2009). "Microseismicity but no tremor accompanying slow slip in the Hikurangi subduction zone, New Zealand". In: *Earth and Planetary Science Letters* 277.1-2, pp. 21–28.

Ghosh, Abhijit et al. (2015). "Very low frequency earthquakes in Cascadia migrate with tremor". In: *Geophysical Research Letters* 42.9, pp. 3228–3232.

Gomberg, J, NM Beeler, et al. (1998). "Earthquake triggering by transient and static deformations". In: *Journal of Geophysical Research: Solid Earth* 103.B10, pp. 24411–24426.

Gomberg, J, PA Reasenberg, et al. (2001). "Earthquake triggering by seismic waves following the Landers and Hector Mine earthquakes". In: *Nature* 411.6836, pp. 462–466.

Gonzalez-Huizar, Hector et al. (2012). "Remote triggered seismicity caused by the 2011, M9. 0 Tohoku-Oki, Japan earthquake". In: *Geophysical research letters* 39.10.

Hill, David P (2008). "Dynamic stresses, Coulomb failure, and remote triggering". In: *Bulletin of the Seismological Society of America* 98.1, pp. 66–92.

Klein, Fred W (2002). *User's guide to HYPOINVERSE-2000, a Fortran program to solve for earthquake locations and magnitudes*. Tech. rep. US Geological Survey.

Love, Augustus Edward Hough (2013). *A treatise on the mathematical theory of elasticity*. Cambridge university press.

Mahesh, P et al. (2013). "One-dimensional reference velocity model and precise locations of earthquake hypocenters in the Kumaon–Garhwal himalaya". In: *Bulletin of the Seismological Society of America* 103.1, pp. 328–339.

Pankow, Kris L et al. (2004). "Triggered seismicity in Utah from the 3 November 2002 Denali fault earthquake". In: *Bulletin of the Seismological Society of America* 94.6B, S332–S347.

Peng, Zhigang and Joan Gomberg (2010). "An integrated perspective of the continuum between earthquakes and slow-slip phenomena". In: *Nature geoscience* 3.9, pp. 599–607.

Prejean, SG et al. (2004). "Remotely triggered seismicity on the United States west coast following the M w 7.9 Denali fault earthquake". In: *Bulletin of the Seismological Society of America* 94.6B, S348–S359.

Prejean, Stephanie G, David P Hill, and RA Myers (2010). "Earthquakes dynamic triggering of". In: *Extreme Environmental Events: Complexity in Forecasting and Early Warning. Springer. Heidelberg*, pp. 425–446.

Rajendran, CP and Kusala Rajendran (2005). "The status of central seismic gap: a perspective based on the spatial and temporal aspects of the large Himalayan earthquakes". In: *Tectonophysics* 395.1-2, pp. 19–39.

Smith, Emily F and Joan Gomberg (2009). "A search in strainmeter data for slow slip associated with triggered and ambient tremor near Parkfield, California". In: *Journal of Geophysical Research: Solid Earth* 114.B12.

Thomas, Trevor W et al. (2013). "Evidence for tidal triggering of high-amplitude rapid tremor reversals and tremor streaks in northern Cascadia". In: *Geophysical research letters* 40.16, pp. 4254–4259.

Van Der Elst, Nicholas J and Emily E Brodsky (2010). "Connecting near-field and far-field earthquake triggering to dynamic strain". In: *Journal of Geophysical Research: Solid Earth* 115.B7.

Van Der Elst, Nicholas J and Heather M Savage (2015). "Frequency dependence of delayed and instantaneous triggering on laboratory and simulated faults governed by rate-state friction". In: *Journal of Geophysical Research: Solid Earth* 120.5, pp. 3406–3429.

Vidale, John E et al. (2011). "Tiny intraplate earthquakes triggered by nearby episodic tremor and slip in Cascadia". In: *Geochemistry, Geophysics, Geosystems* 12.6.

Waldhauser, Felix and William L Ellsworth (2000). "A double-difference earthquake location algorithm: Method and application to the northern Hayward fault, California". In: *Bulletin of the Seismological Society of America* 90.6, pp. 1353–1368.

Zhang, Jian et al. (2011). "Cascadia tremor spectra: Low corner frequencies and earthquake-like high-frequency falloff". In: *Geochemistry, Geophysics, Geosystems* 12.10.

Chapter 5

Conclusions

Since the onset of collision between the Indian and Eurasian plates 50 Ma, the Himalayas have been faulting a folding, producing many of the largest mountains and earthquakes in the world. Along this active margin reside millions of people, marking the Himalayas as not only a place of great scientific interest, but also one that poses a high societal risk. Seismological studies are therefore imperative to probing the complex system of active faults and related deformation processes along different segments of the Himalayas. Only in recent decades have well-distributed seismic networks been deployed to offer a contemporary snapshot into Himalayan tectonic processes that began long ago (e.g., Karplus et al., 2020; Sheehan et al., 2008; Mahesh et al., 2013). Since then, our understanding of the Himalayas has been rapidly growing and evolving. In the following, we provide a summary of this dissertation's findings and subsequent contributions to the relevant scientific literature, and briefly discuss what more work needs to be done going forward.

As discussed earlier, the bulk of Himalayan seismicity appears as a band of small to moderate sized earthquakes that manifest above the décollement within the Lesser Himalaya. This band of constant seismic activity resides in the transition zone between up-dip locked and down-dip creeping (i.e. aseismic) segments of the MHT (Ader et al., 2012). The surface expression of active deformation processes in this area are reflected directly above by the dramatic increase in topography from the Lesser to Higher Himalaya. For a long time seismic observations have been in pursuit of capturing these earthquakes to identify structures, their geometries, and how they are influencing the behavior of large damaging earthquakes. However, detecting small earthquakes—those of which that offer crucial insight into the finer structural features—and determining their hypocentral locations with high accuracy, is challenging. This can result in a largely incomplete earthquake catalog that makes it difficult to discern the locations and geometries of faults, especially in depth profiles. That said, the two seismic network datasets used in this dissertation provided an opportunity (and example) whereupon robust observations can be made. Thanks to close station spacing and their broad distribution from the Sub-to-Higher Himalaya, both networks captured a wide range of earthquake magnitudes and made it possible to obtain well-constrained hypocentral estimates. These earthquake catalogs representing two spatially distinct areas along the Himalayan arc share many similarities, yet some differences, that we summarize in the following ways.

At shallow depths (<25 km), in map view, both catalogs show a dense band of seismicity roughly trending NW-SE within the Lesser Himalaya. Since the 2015 Mw 7.8 Gorkha earthquake, the NAMASTE network captured thousands more earthquakes

(aftershocks) than the (ambient) seismicity captured by the Uttarakhand network. This stark contrast effectively demonstrates the MHT being at different time periods in their earthquake cycle: the post-seismic (central Nepal) and inter-seismic (Uttarakhand) periods. At depth, both catalogs exhibit the majority of seismicity to be occurring on moderately-to-steeply dipping fault structures. In central Nepal, from the pattern of seismicity and focal mechanisms, we infer at least three active and imbricate faults that belong to a Lesser Himalaya duplex. Since the aftershocks also illuminate the sub-horizontal (flat) portions of the MHT, we provide a more refined model of its geometry by embedding a duplex-like architecture. In Uttarakhand, we delineate at least two imbricate faults in proximity to the 1999 Mw 6.5 Chamoli earthquake, and also infer here that a duplex structure was likely (re)activated. However, due to the lower level of seismicity that is detected, we are unable to properly constrain the location and geometry of the MHT in this area directly. We then rely on the MHT profile inferred by Caldwell et al. (2013), who used receiver functions to image crustal features and the Moho using the same data set. When combining our interpretations with Caldwell et al.'s, we construct a more refined model of the MHT in Uttarakhand; where instead of a major "ramp" connecting the upper and lower flat segments of the MHT, as Caldwell et al. (2013) show, we infer a duplex. This MHT model closely resembles the one we derive for central Nepal, suggesting that this structural feature exists in multiple areas along the Himalayan arc. As various types of models have shown (e.g., Dal Zilio et al., 2019; Hubbard et al., 2016; J. Mugnier et al., 1997; Srivastava and Mitra, 1994), growth of a duplex is initiated by the presence of a ramp along the MHT, beneath the junction of the Lesser and Higher Himalaya. The contemporary ramp likely acts as part of the sole

thrust for the duplex, containing within it multiple imbricate thrusts (i.e. older ramps) that splay off the MHT and are bounded above by a sub-horizontal roof thrust. Since geodetic strain measurements show variability along the arc (Ader et al., 2012), it can be conjectured that a duplex structure exists along the arc in varying degrees of development; for example, a young duplex might contain two active thrusts, whereas an older duplex might contain three—as exhibited in our Uttarakhand and central Nepal datasets, respectively. This could then partly explain why geological studies have inferred duplex structures in some areas of the Himalayas and not in others: a mature duplex may have developed sufficent thrusts to stack or "pile up" relatively soft Lesser Himalayan rock, resulting in its surface expression as an exhumed and unroofed (eroded) antiform, exposing the thrust sheets at its core (e.g., Srivastava and Mitra, 1994; DeCelles et al., 2001; J.-L. Mugnier et al., 2017). Whether a duplex structure is prominent throughout the Himalayas or only in certain areas, it can be viewed as an impediment to plate convergence, and elucidate how the arc is deforming and supporting the world's largest mountain range. Further, if a duplex developmentally varies along strike, it could be contributing to the structural segmentation along the MHT, as demarcated from inferred rupture zones of large historic earthquakes. Those areas of significant structural heterogeneity (or "barriers") could be indicative of high stress concentrations and, at least partly, be associated with the timing and rupture process of earthquakes that nucleate on the MHT—including those pending within the central seismic gap.

Perhaps the biggest difference between the two earthquake catalogs presented here is the abundance of seismicity taking place down to near-Moho depths beneath Uttarakhand,

and the virtual absence of them beneath central Nepal. Exploring the range of possibilities for this disparity is beyond the scope of this dissertation, so for now we only investigate their occurrence beneath Uttarakhand. As discussed in the third chapter, it is argued that the strength of the lithosphere resides in the Earth's crust, making the general observation of seismicity occurring at and below the Moho more dubious. This especially applies to the deep seismicity observed beneath the Lesser and Higher Himalaya, where the subducting Indian plate is still too buoyant to plunge steeply into the mantle—unlike typical oceanic-continental subduction zone settings (e.g., the Wadati-Benioff zone; Smalley Jr and Isacks, 1987). To reconcile this observation, we carefully select ten earthquakes that have well-constrained location estimates, and were deemed to be reliable for further examination. For those ten, small magnitude earthquakes, we compute their focal mechanisms to understand how brittle deformation is occurring with respect to varying conditions expected above and below the Moho, and laterally along the Indian lithosphere. We obtain an assortment of focal mechanisms representing various faulting styles, with most of them indicating normal faulting to be the predominant style of deformation at this location. Other modeling and seismological studies carried out elsewhere along the arc indicate that flexural bending of the Indian lithosphere is taking place where our ten examined earthquakes are located—directly beneath the Himalayas. While the diverse set of focal mechanisms we obtain might indicate small-scale heterogeneities, or dynamic lithospheric processes (such as underplating), further analysis in needed before offering a firm explanation for the existence of deep earthquakes beneath Uttarakhand.

Lastly, apart from central Nepal after the Gorkha earthquake, the comparatively low seismicity rate in Uttarakhand allowed us to capture the first observation of dynamic and delayed remote earthquake triggering in the Himalayas. Within minutes after the 2006 Mw 8.5 Sumatra earthquake, its low-frequency high amplitude surface waves arrived ∼4,500 km away in Uttarakhand, and prompted a rapid onset heightened seismicity that lasted for a week. The dramatic increase in seismicity after the passage of the teleseismic wave train, with respect to the average seismicity rate prior, suggests that this observation is likely not a coincidence initiated from local tectonic processes. We use a simple 1-D measurement to estimate the amount of dynamic stress imparted by the peak amplitude of the passing surface waves. This measurement is in agreement with those taken from other documented instances of dynamic triggering that occurred across different tectonic settings. Our analysis in Chapter 4 reaffirms the notion that faults in the central seismic gap are critically stressed and highly sensitive to small, transient stress perturbations.

The seismological investigations carried out in this dissertation contributes just a portion of the substantial progress made in recent decades towards our understanding of Himalayan seismotectonics and seismogenesis; however, considerable more work remains. At both ends of the central seismic gap—in central Nepal and Uttarakhand—we provide evidence of a duplex structure through high-resolution imaging of active faults mapped by the earthquakes themselves, and in turn derive a more refined geometry model of the MHT. Similar seismic experiments and analyses need to be carried out in other segments of the Himalaya to assess the extent to which a duplex is present, and developed, along the arc. If it does indeed have a pervasive presence, geological and geophysical models

that investigate deformation and earthquake processes in this tectonic setting should be updated accordingly. The two simple MHT geometry models constructed here can be a good starting point to investigate the controls that a duplex architecture has on those processes. With regards to the deep seismicity observed beneath Uttarakhand, performing waveform template matching on our ten high-quality earthquakes to detect more occurring at similar depths, would further substantiate the postulation that the strength of the Indian lithosphere is cable of extending to the Moho or beyond. Further tests to validate the hypocentral location of those deeper earthquakes would still be needed to make a stronger argument. If they are indeed abundant, real, and accurate at those depths, a systematic examination of their source parameters (i.e. from focal mechanisms) would be helpful when exploring the possible range of conditions giving rise to them. Further, those earthquakes could be used to perform seismic tomography techniques (e.g., with TomoDD; Zhang and Thurber, 2003) to create 2-D or 3-D images of deep structural features. This would provide additional resolution and constraint on features (e.g. Moho) that have been identified beneath the Himalayas so far using other imaging techniques, such as receiver function stacking (e.g., Nábělek et al., 2009; Schulte-Pelkum et al., 2005; Caldwell et al., 2013). On another note, the earthquake triggering phenomenon in Uttarakhand could be examined further. In this dissertation we only perform a cursory investigation into a single instance of local earthquakes triggered by a large distant teleseismic event. Not mentioned earlier, we also infer other (albeit less obvious) time periods in which a teleseismic event likely triggered local seismicity. Discerning why only certain teleseismic events trigger heightened seismicity in Uttarakhand, while many others do not, can provide valuable insight into the

specific physical conditions that drive this phenomenon in general. At the same time, a detailed examination into earthquake triggering in Uttarakhand could be used as a proxy to learn more about how earthquakes nucleate and rupture along the MHT, and influence one another in the Himalayas.

Bibliography

Ader, Thomas et al. (2012). "Convergence rate across the Nepal Himalaya and interseismic coupling on the Main Himalayan Thrust: Implications for seismic hazard". In: *Journal of Geophysical Research: Solid Earth* 117.B4.

Caldwell, Warren B et al. (2013). "Characterizing the Main Himalayan Thrust in the Garhwal Himalaya, India with receiver function CCP stacking". In: *Earth and Planetary Science Letters* 367, pp. 15–27.

Dal Zilio, Luca et al. (2019). "Bimodal seismicity in the Himalaya controlled by fault friction and geometry". In: *Nature communications* 10.1, pp. 1–11.

DeCelles, Peter G et al. (2001). "Stratigraphy, structure, and tectonic evolution of the Himalayan fold-thrust belt in western Nepal". In: *Tectonics* 20.4, pp. 487–509.

Hubbard, Judith et al. (2016). "Structural segmentation controlled the 2015 Mw 7.8 Gorkha earthquake rupture in Nepal". In: *Geology* 44.8, pp. 639–642.

Karplus, Marianne S et al. (2020). "A rapid response network to record aftershocks of the 2015 M 7.8 Gorkha earthquake in Nepal". In: *Seismological Research Letters* 91.4, pp. 2399–2408.

Mahesh, P et al. (2013). "One-dimensional reference velocity model and precise locations of earthquake hypocenters in the Kumaon–Garhwal himalaya". In: *Bulletin of the Seismological Society of America* 103.1, pp. 328–339.

Mugnier, Jean-Louis et al. (2017). "Segmentation of the Himalayan megathrust around the Gorkha earthquake (25 April 2015) in Nepal". In: *Journal of Asian Earth Sciences* 141, pp. 236–252.

Mugnier, JL et al. (1997). "Thrust geometry controlled by erosion and sedimentation: A view from analogue models". In: *Geology* 25.5, pp. 427–430.

Nábělek, John et al. (2009). "Underplating in the Himalaya-Tibet collision zone revealed by the Hi-CLIMB experiment". In: *Science* 325.5946, pp. 1371–1374.

Schulte-Pelkum, Vera et al. (2005). "Imaging the Indian subcontinent beneath the Himalaya". In: *Nature* 435.7046, pp. 1222–1225.

Sheehan, Anne F et al. (2008). "Earthquakes and crustal structure of Himalaya from Himalayan Nepal-Tibet seismic experiment (HIMNT)". In: *Journal of Nepal Geological Society* 38, pp. 1–8.

Smalley Jr, Robert F and Bryan L Isacks (1987). "A high-resolution local network study of the Nazca Plate Wadati-Benioff Zone under western Argentina". In: *Journal of Geophysical Research: Solid Earth* 92.B13, pp. 13903–13912.

Srivastava, Praveen and Gautam Mitra (1994). "Thrust geometries and deep structure of the outer and lesser Himalaya, Kumaon and Garhwal (India): Implications for evolution of the Himalayan fold-and-thrust belt". In: *Tectonics* 13.1, pp. 89–109.

Zhang, Haijiang and Clifford Thurber (2003). "User's manual for tomoDD1. 1 (double-difference tomography) for determining event locations and velocity structure from local earthquakes and explosions". In: *Department of Geology and Geophysics, University of Wisconsin-Madison, Madison, WI.*